FINITE ELEMENT MODEL

Governing Equation

The heat transfer in the biological tissue is governed by the well-known Penne bio-heat equation.

$$c\rho\frac{\partial T}{\partial t} = \left\{\frac{\partial}{\partial x}\left(k\frac{\partial T}{\partial x}\right) + \frac{\partial}{\partial y}\left(k\frac{\partial T}{\partial y}\right) + \omega_b\rho_b c_b(T_a - T)\right\} \quad (1)$$

where *c, ρ* and *k* are the specific heat, density and thermal conductivity of the tissue respectively, ρ_b, c_b denote density and specific heat of blood; ω_b the blood perfusion; T_a the known arterial temperature, T is unknown tissue temperature, and the metabolic heat generation has been considered to be negligible due to the fact that temperature change caused by heating disk is much more higher than metabolic hear generation.

The simplified form of Eq. (3.1) can be expressed as

$$c\rho\frac{\partial T}{\partial t} = \left\{\frac{\partial}{\partial x}\left(k\frac{\partial T}{\partial x}\right) + \frac{\partial}{\partial y}\left(k\frac{\partial T}{\partial y}\right) - CT + f\right\} \quad (2)$$

Where $C = \omega_b\rho_b c_b$ and $f = CT_a$

3.2 Development of Weak Form

The weak form of the differential equation (Applying Weighted Residual Method) is derived as

$$0 = \int_{\Omega} w\left[\rho c\frac{\partial T}{\partial t} - \left\{\frac{\partial}{\partial x}\left(k\frac{\partial T}{\partial x}\right) + \frac{\partial}{\partial y}\left(k\frac{\partial T}{\partial y}\right)\right\} + CT - f\right]dxdy$$

Applying gradient (Divergence theorem)

$$\int_{\Omega} -w\frac{\partial}{\partial x}\left(k\frac{\partial T}{\partial x}\right)dxdy = \int_{\Omega} k\frac{\partial w}{\partial x}\frac{\partial T}{\partial x}dxdy - \oint_{\Gamma} wk\frac{\partial T}{\partial x}\eta_x ds$$

$$\int_{\Omega} -w\frac{\partial}{\partial y}\left(k\frac{\partial T}{\partial y}\right)dxdy = \int_{\Omega} k\frac{\partial w}{\partial y}\frac{\partial T}{\partial y}dxdy - \oint_{\Gamma} wk\frac{\partial T}{\partial y}\eta_y ds$$

Weak form of the equation:

$$0 = \int_{\Omega}\left[w\rho c\frac{\partial T}{\partial t} + k\frac{\partial w}{\partial x}\frac{\partial T}{\partial x} + k\frac{\partial w}{\partial y}\frac{\partial T}{\partial y} + CwT - wf\right]dxdx - w\oint_{\Gamma}\left(k\frac{\partial T}{\partial x}\eta_x + k\frac{\partial T}{\partial y}\eta_y\right)ds$$

For convective boundary, the natural boundary condition is a balance of energy transfer across the boundary due to conduction and/ or convection (i.e., Newton's law of cooling):

$$k\frac{\partial T}{\partial x}\eta_x + k\frac{\partial T}{\partial y}\eta_y + \beta(T - T_{\infty}) = \hat{q}_n$$

where β is the convective conductance (or the convective heat transfer coefficient in W $m^{-20}C^{-1}$), T_{∞} is the ambient temperature, and $\hat{q}_n$ is the specific heat flow. The first two terms account for heat transfer by conduction, the third term for heat transfer by convection, while the term on the right hand side accounts for specific heat flux. The boundary integral should be modified to account for the convective heat transfer term. We use in the weak form ($\hat{q}_n$ is replaced by q_n , which is obtained on the element boundary).

$$0 = \int_{\Omega}[w\rho c\frac{\partial T}{\partial t} + k\frac{\partial w}{\partial x}\frac{\partial T}{\partial x} + k\frac{\partial w}{\partial y}\frac{\partial T}{\partial y} + CwT - wf]dxdy$$

$$-w\oint_{\Gamma}[q_n - \beta(T - T_{\infty})]ds \qquad (3)$$

$$= B(w,T) - l(w)$$

Where w is the weight function, and $B(.,.)$ and $l(.)$ are the bilinear and linear forms

$$B(w,T) = \int_{\Omega}\left[w\rho c\frac{\partial T}{\partial t} + k\frac{\partial w}{\partial x}\frac{\partial T}{\partial x} + k\frac{\partial w}{\partial y}\frac{\partial T}{\partial y} + CwT\right]dxdy + \oint_{\Gamma}\beta wTds$$

$$l(w) = \int_{\Omega} wfdxdy + \oint_{\Gamma}\beta wT_{\infty}ds + \oint_{\Gamma} wq_n ds$$

3.2.1 Linear Approximation

Rectangular Element

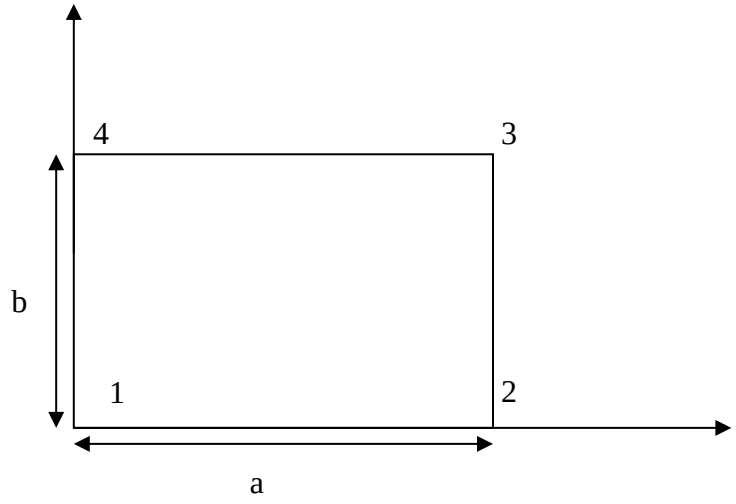

$$T = \sum_{j=1}^{4} T_j^e \psi_j^e(x,y)$$

$$\psi_1^e = (1-\frac{x}{a})(1-\frac{y}{b}) \qquad \psi_2^e = \frac{x}{a}(1-\frac{y}{b}) \qquad \psi_3^e = \frac{x}{a}\frac{y}{b} \qquad \psi_1^e = (1-\frac{x}{a})\frac{y}{b}$$

Here

$$[C_{ij}^e] = \frac{1}{36}\rho Cab\begin{bmatrix} 4 & 2 & 1 & 2 \\ 2 & 4 & 2 & 1 \\ 1 & 2 & 4 & 2 \\ 2 & 1 & 2 & 4 \end{bmatrix} \qquad [H_{ij}^e] = \frac{1}{4}hb\begin{bmatrix} 2 & 0 & 0 & 1 \\ 0 & 0 & 0 & 0 \\ 0 & 0 & 0 & 0 \\ 1 & 0 & 0 & 2 \end{bmatrix}$$

$$[f_i^e] = \frac{1}{4}ab[1 \quad 1 \quad 1 \quad 1] \qquad [p_i^e] = \frac{1}{2}bhT_\infty[1 \quad 0 \quad 0 \quad 1]$$

Matrix Assembly:

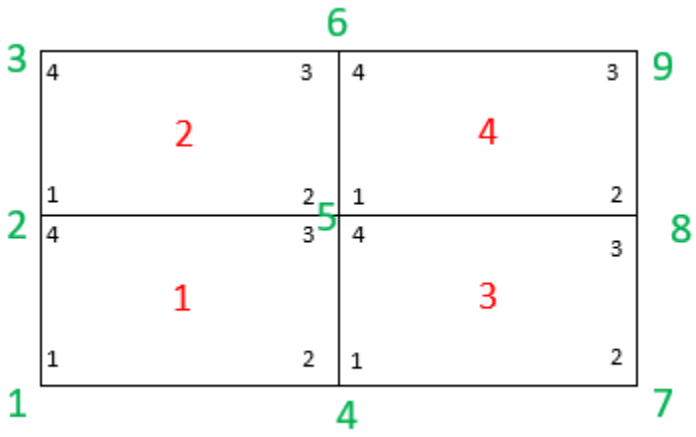

K^1_{11}	K^1_{14}	0	K^1_{12}	K^1_{13}	0	0	0	0
K^1_{41}	$K^3_{11}+K^1_{44}$	K^3_{41}	K^1_{42}	$K_{43}+k_{12}$	K^2_{13}	0	0	0
0	K^3_{41}	K44	0	K^2_{42}	K^2_{43}	0	0	0
K^1_{12}	K^1_{42}	0	$K^1_{22}+k^3_{11}$	$K^3_{41}+K^1_{23}$	0	K^3_{12}	K^3_{13}	0
K^1_{13}	$K^1_{43}+K^2_{12}$	K^2_{42}	$K^3_{41}+K^1_{23}$	$K^4_{11}+k^3_{44}+K^1_{33}+k^2_{22}$	$K^4_{14}+K^2_{23}$	K^3_{42}	$K^4_{12}+K^3_{43}$	K^4_{13}
0	K^2_{13}	K^2_{43}	0	$K^2_{23}+K^4_{14}$	$K^4_{44}+K^3_{33}$	0	K^4_{42}	K^4_{43}
0	0	0	K^3_{12}	K^3_{42}	0	K^3_{22}	K^3_{23}	0
0	0	0	K^3_{13}	$K^4_{12}+K^3_{43}$	K^4_{42}	K^3_{23}	$K^4_{22}+K^3_{33}$	K^4_{23}
0	0	0	0	K^4_{13}	K^4_{43}	0	K^4_{23}	K^4_{33}

F^1_1	$F^1_4+F^2_1$	F^2_4	$F^1_2+F^3_1$	$F^1_3+F^2_2+F^3_4+F^4_1$	$F^2_3+F^4_4$	F^3_2	$F^3_3+F^4_2$	F^4_3

Linear triangular element

$$T = \sum_{j=1}^{3} T_j^e \psi_j^e(x, y)$$

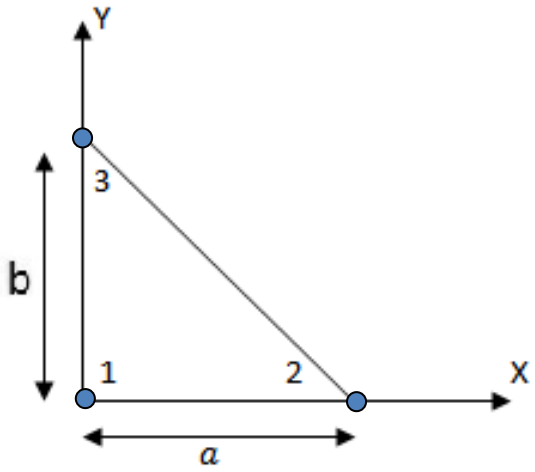

Figure 1.1 Linear triangular Element

where, $\psi_1^e = 1 - \frac{x}{a} - \frac{y}{b}$ $\psi_2^e = \frac{x}{a}$ $\psi_3^e = \frac{y}{b}$

Quadratic Approximation

Considering quadratic triangular element as finite element we take quadratic approximation as

$$T = \sum_{j=1}^{6} T_j^e \psi_j^e(x, y)$$

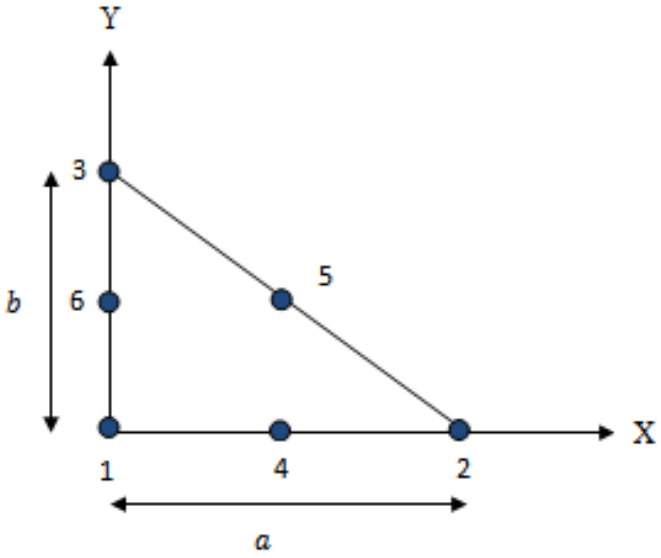

Figure 1.2 Quadratic triangular Element

where,

$$\psi_1^e = \left(1 - \frac{x}{a} - \frac{y}{b}\right)\left(1 - \frac{2x}{a} - \frac{2y}{b}\right)$$

$$\psi_2^e = \frac{2x^2 - ax}{a^2}$$

$$\psi_3^e = \frac{2y^2 - by}{b^2}$$

$$\psi_4^e = \frac{4x}{a}\left(1 - \frac{x}{a} - \frac{y}{b}\right)$$

$$\psi_5^e = \frac{4xy}{ab}$$

$$\psi_6^e = \frac{4y}{b}(1 - \frac{x}{a} - \frac{y}{b})$$

3.3 Finite Element Model

We substitute the finite element approximation of the form

$T = \sum_{j=1}^{n} T_j^e \psi_j^e(x, y)$ for T and ψ_i^e for $w$into (3.3)

$$0 = \int_{\Omega^e} \rho c \psi_i^e \psi_j^e \frac{\partial T_j^e}{\partial t} dxdy$$

$$+ \int_{\Omega^e} \left[\left\{k \frac{\partial \psi_i^e}{\partial x}\frac{\partial \psi_j^e}{\partial x} + k \frac{\partial \psi_i^e}{\partial y}\frac{\partial \psi_j^e}{\partial y} + C\psi_i^e \psi_j^e\right\} dxdy + \oint_{\Gamma^e} \beta \psi_i^e \psi_j^e ds\right] T_j^e$$

$$- \int_{\Omega^e} f\psi_i^e dxdy - \oint_{\Gamma} \psi_i^e \beta T_\infty ds - \oint_{\Gamma} \psi_i^e q_n ds$$

The finite element model of the governing equation is

$$0 = \sum_{j=1}^{n} \left\{ \int_{\Omega^e} \rho c \psi_i^e \psi_j^e \frac{\partial T_j^e}{\partial t} dxdy + \int_{\Omega^e} \left[\left\{ k \frac{\partial \psi_i^e}{\partial x} \frac{\partial \psi_j^e}{\partial x} + k \frac{\partial \psi_i^e}{\partial y} \frac{\partial \psi_j^e}{\partial y} + C \psi_i^e \psi_j^e \right\} dxdy + \oint_{\Gamma^e} \beta \psi_i^e \psi_j^e ds \right] T_j^e - \int_{\Omega^e} f \psi_i^e dxdy - \oint_{\Gamma} \psi_i^e \beta T_\infty ds - \oint_{\Gamma} \psi_i^e q_n ds \right\} \quad (3.4)$$

Simplifying Eq. (3.4) we get

$$0 = \sum_{j=1}^{n} \left\{ C_{ij}^e \dot{T}_j^e + \left[K_{ij}^e + H_{ij}^e \right] T_j^e - q_i^e - Q_i^e - P_i^e \right\}$$

where,

$$C_{ij}^e = \int_{\Omega^e} \rho c \psi_i^e \psi_j^e dxdy$$

$$K_{ij}^e = \int_{\Omega^e} \left\{ k \frac{\partial \psi_i^e}{\partial x} \frac{\partial \psi_j^e}{\partial x} + k \frac{\partial \psi_i^e}{\partial y} \frac{\partial \psi_j^e}{\partial y} + C \psi_i^e \psi_j^e \right\} dxdy$$

$$H_{ij}^e = \oint_{\Gamma^e} \beta \psi_i^e \psi_j^e ds$$

$$q_j^e = \int_{\Omega^e} f \psi_i^e dxdy$$

$$P_i^e = \oint_{\Gamma} \psi_i^e q_n ds$$

$$Q_i^e = \oint_{\Gamma} \psi_i^e \beta T_\infty ds$$

In matrix notation the finite element model can be expressed as

$$[C]\{\dot{T}\} + [K]\{T\} = \{Q\} + \{q\} + \{P\} \quad (3.5)$$

where, [C] is the capacitance matrix , [K] is the conductivity matrix and right hand side is a vector.

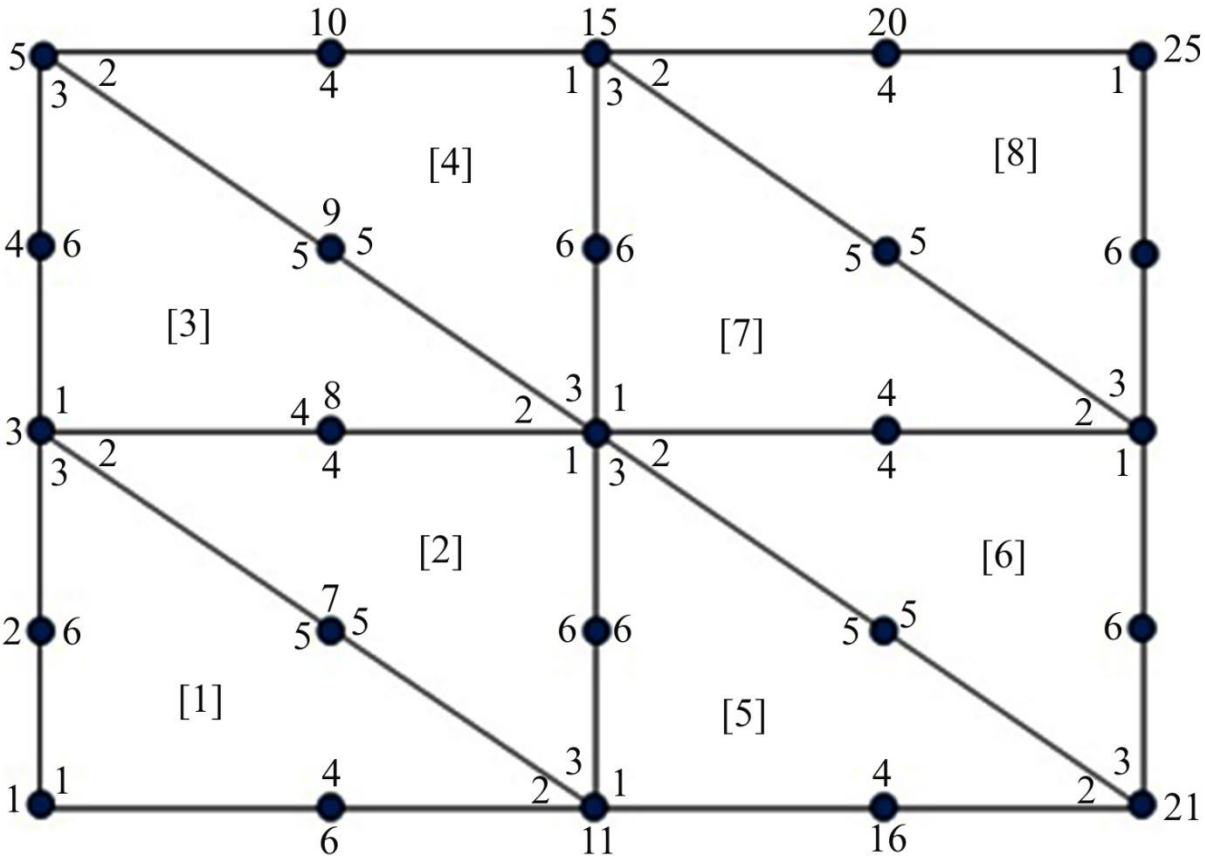

Figure 1.3 Mesh generation of quadratic triangular element.

Now we assemble the matrices in a sample domain in Fig. 3.3 for quadratic triangular element.

For element [1]:

$$C_{ij}^{e} = \int_{\Omega^e} \rho c \psi_i^e \psi_j^e \, dxdy$$

$$C_{11} = \rho c \iint \psi_1 \psi_1 dxdy$$

$$C_{11} = \rho c \int_0^a \int_0^{(ab-bx)/a} \left\{\left(1 - \frac{x}{a} - \frac{y}{b}\right)\left(1 - \frac{2x}{a} - \frac{2y}{b}\right)\right\}^2 dxdy$$

$$= \frac{ab}{60}\rho c$$

$$C_{12} = \rho c \int_0^a \int_0^{(ab-bx)/a} \left(1 - \frac{x}{a} - \frac{y}{b}\right)\left(1 - \frac{2x}{a} - \frac{2y}{b}\right)\left(\frac{2x^2 - ax}{a^2}\right) dxdy$$

$$= -\frac{ab}{360}\rho c = C_{21}$$

$$C_{13} = \rho c \int_0^a \int_0^{(ab-bx)/a} \left(1 - \frac{x}{a} - \frac{y}{b}\right)\left(1 - \frac{2x}{a} - \frac{2y}{b}\right)\left(\frac{2y^2 - by}{b^2}\right) dxdy$$

$$= -\frac{ab}{360}\rho c = C_{31}$$

$$C_{14} = \rho c \int_0^a \int_0^{(ab-bx)/a} \left(1 - \frac{x}{a} - \frac{y}{b}\right)\left(1 - \frac{2x}{a} - \frac{2y}{b}\right)\frac{4x}{a}\left(1 - \frac{x}{a} - \frac{y}{b}\right) dxdy$$

$$= 0 = C_{41}$$

$$C_{15} = \rho c \int_0^a \int_0^{(ab-bx)/a} \left(1 - \frac{x}{a} - \frac{y}{b}\right)\left(1 - \frac{2x}{a} - \frac{2y}{b}\right)\frac{4xy}{ab} dxdy$$

$$= -\frac{ab}{90}\rho c = C_{51}$$

$$C_{16} = \rho c \int_0^a \int_0^{(ab-bx)/a} \left(1 - \frac{x}{a} - \frac{y}{b}\right)\left(1 - \frac{2x}{a} - \frac{2y}{b}\right)\frac{4y}{b}\left(1 - \frac{x}{a} - \frac{y}{b}\right) dxdy$$

$$= 0 = C_{61}$$

$$C_{22} = \rho c \int_0^a \int_0^{(ab-bx)/a} \left(\frac{2x^2 - ax}{a^2}\right)\left(\frac{2x^2 - ax}{a^2}\right) dxdy$$

$$= \frac{ab}{60}\rho c$$

$$C_{23} = \rho c \int_0^a \int_0^{(ab-bx)/a} \left(\frac{2x^2 - ax}{a^2}\right)\left(\frac{2y^2 - by}{b^2}\right) dxdy$$

$$= -\frac{ab}{360}\rho c = C_{32}$$

$$C_{24} = \rho c \int_0^a \int_0^{(ab-bx)/a} \left(\frac{2x^2 - ax}{a^2}\right)\frac{4x}{a}\left(1 - \frac{x}{a} - \frac{y}{b}\right) dxdy = 0 = C_{42}$$

$$C_{25} = \rho c \int_0^a \int_0^{(ab-bx)/a} \left(\frac{2x^2 - ax}{a^2}\right)\frac{4xy}{ab} dxdy = 0 = C_{52}$$

$$C_{26} = \rho c \int_0^a \int_0^{(ab-bx)/a} \left(\frac{2x^2 - ax}{a^2}\right)\frac{4y}{b}\left(1 - \frac{x}{a} - \frac{y}{b}\right) dxdy = -\frac{ab}{90}\rho c = C_{62}$$

$$C_{33} = \rho c \int_0^a \int_0^{(ab-bx)/a} \left(\frac{2y^2 - bx}{b^2}\right)\left(\frac{2y^2 - by}{b^2}\right) dxdy = \frac{ab}{60}\rho c$$

$$C_{34} = \rho c \int_0^a \int_0^{(ab-bx)/a} \left(\frac{2y^2 - bx}{b^2}\right)\frac{4x}{a}\left(1 - \frac{x}{a} - \frac{y}{b}\right) dxdy = -\frac{ab}{90}\rho c = C_{43}$$

$$C_{35} = \rho c \int_0^a \int_0^{(ab-bx)/a} \left(\frac{2y^2 - bx}{b^2}\right)\frac{4xy}{ab} dxdy = 0 = C_{53}$$

$$C_{36} = \rho c \int_0^a \int_0^{(ab-bx)/a} \left(\frac{2y^2 - bx}{b^2}\right)\frac{4y}{b}\left(1 - \frac{x}{a} - \frac{y}{b}\right) dxdy = 0 = C_{63}$$

similarly,

$C_{44} = \frac{4ab}{45}\rho c$; $C_{45} = C_{54} = \frac{2ab}{45}\rho c$; $C_{46} = C_{64} = \frac{2ab}{45}\rho c$;

$C_{55} = \frac{4ab}{45}\rho c$; $C_{56} = C_{65} = \frac{2ab}{45}\rho c$;

$C_{66} = \frac{4ab}{45}\rho c$.

Now

$$K_{ij}^e = \int_{\Omega^e} \left[\left\{ k \frac{\partial \psi_i^e}{\partial x} \frac{\partial \psi_j^e}{\partial x} + k \frac{\partial \psi_i^e}{\partial y} \frac{\partial \psi_j^e}{\partial y} \right\} + C \psi_i^e \psi_j^e \right] dxdy = M_{ij} + N_{ij}$$

where ,

$$M_{ij} = k \iint \frac{\partial \psi_i^e}{\partial x} \frac{\partial \psi_j^e}{\partial x} + \frac{\partial \psi_i^e}{\partial y} \frac{\partial \psi_j^e}{\partial y} dxdy$$

and

$$N_{ij} = C \iint \psi_i^e \psi_j^e dxdy$$

$$M_{11} = k \int_0^a \int_0^{(ab-bx)/a} \frac{\partial \psi_1}{\partial x} \frac{\partial \psi_1}{\partial x} + \frac{\partial \psi_1}{\partial y} \frac{\partial \psi_1}{\partial y} dxdy$$

$$= k \iint [\frac{\partial}{\partial x} \frac{\partial}{\partial x} \{\}$$

$$+ \frac{\partial}{\partial y} \{ \left(1 - \frac{x}{a} - \frac{y}{b}\right) \left(1 - \frac{2x}{a} - \frac{2y}{b}\right) \} \frac{\partial}{\partial y} \{ \left(1 - \frac{x}{a} - \frac{y}{b}\right) \left(1 - \frac{2x}{a} - \frac{2y}{b}\right) \}] dxdy$$

$$= \frac{k(a^2 + b^2)}{2ab}$$

$$M_{12} = k \iint \frac{\partial \psi_1}{\partial x} \frac{\partial \psi_2}{\partial x} + \frac{\partial \psi_1}{\partial y} \frac{\partial \psi_2}{\partial y} dxdy$$

$$= k \iint [\frac{\partial}{\partial x} \{ \left(1 - \frac{x}{a} - \frac{y}{b}\right) \left(1 - \frac{2x}{a} - \frac{2y}{b}\right) \} \frac{\partial}{\partial x} \left(\frac{2x^2 - ax}{a^2} \right)$$

$$+ \frac{\partial}{\partial y} \{ \left(1 - \frac{x}{a} - \frac{y}{b}\right) \left(1 - \frac{2x}{a} - \frac{2y}{b}\right) \} \frac{\partial}{\partial y} \left(\frac{2x^2 - ax}{a^2} \right)] dxdy$$

$$= \frac{kb}{6a} = M_{21}$$

$$M_{13} = k \iint \frac{\partial \psi_1}{\partial x}\frac{\partial \psi_3}{\partial x} + \frac{\partial \psi_1}{\partial y}\frac{\partial \psi_3}{\partial y}\, dxdy$$

$$= k \iint [\frac{\partial}{\partial x}\{\left(1 - \frac{x}{a} - \frac{y}{b}\right)\left(1 - \frac{2x}{a} - \frac{2y}{b}\right)\}\frac{\partial}{\partial x}\left(\frac{2y^2 - by}{b^2}\right)$$

$$+ \frac{\partial}{\partial y}\{\left(1 - \frac{x}{a} - \frac{y}{b}\right)\left(1 - \frac{2x}{a} - \frac{2y}{b}\right)\}\frac{\partial}{\partial y}\left(\frac{2y^2 - by}{b^2}\right)]dxdy$$

$$= \frac{ka}{6b} = M_{31}$$

$$M_{14} = k \iint \frac{\partial \psi_1}{\partial x}\frac{\partial \psi_4}{\partial x} + \frac{\partial \psi_1}{\partial y}\frac{\partial \psi_4}{\partial y}\, dxdy$$

$$= k \iint [\frac{\partial}{\partial x}\{\left(1 - \frac{x}{a} - \frac{y}{b}\right)\left(1 - \frac{2x}{a} - \frac{2y}{b}\right)\}\frac{\partial}{\partial x}\{\frac{4x}{a}\left(1 - \frac{x}{a} - \frac{y}{b}\right)\}$$

$$+ \frac{\partial}{\partial y}\{\left(1 - \frac{x}{a} - \frac{y}{b}\right)\left(1 - \frac{2x}{a} - \frac{2y}{b}\right)\}\frac{\partial}{\partial y}\{\frac{4x}{a}\left(1 - \frac{x}{a} - \frac{y}{b}\right)\}]dxdy$$

$$= -\frac{2kb}{3a} = M_{41}$$

$$M_{15} = k \iint \frac{\partial \psi_1}{\partial x}\frac{\partial \psi_5}{\partial x} + \frac{\partial \psi_1}{\partial y}\frac{\partial \psi_5}{\partial y}\, dxdy$$

$$= k \iint [\frac{\partial}{\partial x}\{\left(1 - \frac{x}{a} - \frac{y}{b}\right)\left(1 - \frac{2x}{a} - \frac{2y}{b}\right)\}\frac{\partial}{\partial x}\left(\frac{4xy}{ab}\right)$$

$$+ \frac{\partial}{\partial y}\{\left(1 - \frac{x}{a} - \frac{y}{b}\right)\left(1 - \frac{2x}{a} - \frac{2y}{b}\right)\}\frac{\partial}{\partial y}\left(\frac{4xy}{ab}\right)]dxdy$$

$$= 0 = M_{51}$$

$$M_{16} = k\iint \frac{\partial\psi_1}{\partial x}\frac{\partial\psi_6}{\partial x} + \frac{\partial\psi_1}{\partial y}\frac{\partial\psi_6}{\partial y}dxdy$$

$$= k\iint [\frac{\partial}{\partial x}\{\left(1 - \frac{x}{a} - \frac{y}{b}\right)\left(1 - \frac{2x}{a} - \frac{2y}{b}\right)\}\frac{\partial}{\partial x}\{\frac{4y}{b}\left(1 - \frac{x}{a} - \frac{y}{b}\right)\}$$

$$+ \frac{\partial}{\partial y}\{\left(1 - \frac{x}{a} - \frac{y}{b}\right)\left(1 - \frac{2x}{a} - \frac{2y}{b}\right)\}\frac{\partial}{\partial y}\{\frac{4y}{b}\left(1 - \frac{x}{a} - \frac{y}{b}\right)\}]dxdy$$

$$= -\frac{2ka}{3b} = M_{61}$$

$$M_{22} = k\iint \frac{\partial\psi_2}{\partial x}\frac{\partial\psi_2}{\partial x} + \frac{\partial\psi_2}{\partial y}\frac{\partial\psi_2}{\partial y}dxdy$$

$$= k\iint [\frac{\partial}{\partial x}\left(\frac{2x^2-ax}{a^2}\right)\frac{\partial}{\partial x}\left(\frac{2x^2-ax}{a^2}\right)$$

$$+ \frac{\partial}{\partial y}\left(\frac{2x^2 - ax}{a^2}\right)\frac{\partial}{\partial y}\left(\frac{2x^2 - ax}{a^2}\right)]dxdy$$

$$= \frac{kb}{2a}$$

$$M_{23} = k\iint \frac{\partial\psi_2}{\partial x}\frac{\partial\psi_3}{\partial x} + \frac{\partial\psi_2}{\partial y}\frac{\partial\psi_3}{\partial y}dxdy$$

$$= k\iint [\frac{\partial}{\partial x}\left(\frac{2x^2-ax}{a^2}\right)\frac{\partial}{\partial x}\left(\frac{2y^2-by}{b^2}\right)$$

$$+ \frac{\partial}{\partial y}\left(\frac{2x^2 - ax}{a^2}\right)\frac{\partial}{\partial y}\left(\frac{2y^2 - by}{b^2}\right)]dxdy$$

$$= 0 = M_{32}$$

$$M_{24} = k\iint \frac{\partial\psi_2}{\partial x}\frac{\partial\psi_4}{\partial x} + \frac{\partial\psi_2}{\partial y}\frac{\partial\psi_4}{\partial y}dxdy$$

$$= k\iint [\frac{\partial}{\partial x}\left(\frac{2x^2-ax}{a^2}\right)\frac{\partial}{\partial x}\{\frac{4x}{a}\left(1 - \frac{x}{a} - \frac{y}{b}\right)\}$$

$$+\frac{\partial}{\partial y}\left(\frac{2x^2-ax}{a^2}\right)\frac{\partial}{\partial y}\{\frac{4x}{a}\left(1-\frac{x}{a}-\frac{y}{b}\right)\}]dxdy$$

$$= -\frac{2kb}{3a} = M_{42}$$

$$M_{25} = k\iint \frac{\partial\psi_2}{\partial x}\frac{\partial\psi_5}{\partial x} + \frac{\partial\psi_2}{\partial y}\frac{\partial\psi_5}{\partial y}dxdy$$

$$= k\iint [\frac{\partial}{\partial x}\left(\frac{2x^2-ax}{a^2}\right)\frac{\partial}{\partial x}\left(\frac{4xy}{ab}\right)$$

$$+\frac{\partial}{\partial y}\left(\frac{2x^2-ax}{a^2}\right)\frac{\partial}{\partial y}\left(\frac{4xy}{ab}\right)]dxdy$$

$$= 0 = M_{52}$$

$$M_{26} = k\iint \frac{\partial\psi_2}{\partial x}\frac{\partial\psi_6}{\partial x} + \frac{\partial\psi_2}{\partial y}\frac{\partial\psi_6}{\partial y}dxdy$$

$$= k\iint [\frac{\partial}{\partial x}\left(\frac{2x^2-ax}{a^2}\right)\frac{\partial}{\partial x}\{\frac{4y}{b}\left(1-\frac{x}{a}-\frac{y}{b}\right)\}$$

$$+\frac{\partial}{\partial y}\left(\frac{2x^2-ax}{a^2}\right)\frac{\partial}{\partial y}\{\frac{4y}{b}\left(1-\frac{x}{a}-\frac{y}{b}\right)\}]dxdy$$

$$= 0 = M_{62}$$

$$M_{33} = k\iint \frac{\partial\psi_3}{\partial x}\frac{\partial\psi_3}{\partial x} + \frac{\partial\psi_3}{\partial y}\frac{\partial\psi_3}{\partial y}dxdy$$

$$= k\iint [\frac{\partial}{\partial x}\left(\frac{2y^2-by}{b^2}\right)\frac{\partial}{\partial x}\left(\frac{2y^2-by}{b^2}\right)$$

$$+\frac{\partial}{\partial y}\left(\frac{2y^2-by}{b^2}\right)\frac{\partial}{\partial y}\left(\frac{2y^2-by}{b^2}\right)]dxdy$$

$$= \frac{ka}{2b}$$

$$M_{34} = k\iint \frac{\partial\psi_3}{\partial x}\frac{\partial\psi_4}{\partial x} + \frac{\partial\psi_3}{\partial y}\frac{\partial\psi_4}{\partial y}dxdy$$

$$= k\iint [\frac{\partial}{\partial x}\left(\frac{2y^2-by}{b^2}\right)\frac{\partial}{\partial x}\{\frac{4x}{a}\left(1-\frac{x}{a}-\frac{y}{b}\right)\}$$

$$+\frac{\partial}{\partial y}\left(\frac{2y^2-by}{b^2}\right)\frac{\partial}{\partial y}\{\frac{4x}{a}\left(1-\frac{x}{a}-\frac{y}{b}\right)\}]dxdy$$

$$= 0 = M_{43}$$

$$M_{35} = k\iint \frac{\partial\psi_3}{\partial x}\frac{\partial\psi_5}{\partial x} + \frac{\partial\psi_3}{\partial y}\frac{\partial\psi_5}{\partial y}dxdy$$

$$= k\iint [\frac{\partial}{\partial x}\left(\frac{2y^2-by}{b^2}\right)\frac{\partial}{\partial x}\left(\frac{4xy}{ab}\right) + \frac{\partial}{\partial y}\left(\frac{2y^2-by}{b^2}\right)\frac{\partial}{\partial y}\left(\frac{4xy}{ab}\right)]dxdy$$

$$= 0 = M_{53}$$

$$M_{36} = k\iint \frac{\partial\psi_3}{\partial x}\frac{\partial\psi_6}{\partial x} + \frac{\partial\psi_3}{\partial y}\frac{\partial\psi_6}{\partial y}dxdy$$

$$= k\iint [\frac{\partial}{\partial x}\left(\frac{2y^2-by}{b^2}\right)\frac{\partial}{\partial x}\{\frac{4y}{b}(1-\frac{x}{a}-\frac{y}{b})\}$$

$$+\frac{\partial}{\partial y}\left(\frac{2y^2-by}{b^2}\right)\frac{\partial}{\partial y}\{\frac{4y}{b}(1-\frac{x}{a}-\frac{y}{b})\}]dxdy$$

$$= -\frac{2ka}{3b} = M_{63}$$

Similarly,

$M_{44} = \frac{4k(a^2+b^2)}{3ab}$; $M_{45} = M_{54} = -\frac{4ka}{3b}$; $M_{46} = M_{64} = 0$;

$M_{55} = \frac{4k(a^2+b^2)}{3ab}$; $M_{56} = M_{65} = -\frac{4kb}{3a}$;

$M_{66} = \frac{4k(a^2+b^2)}{3ab}$;

Again,

$$N_{11} = C\int_0^a \int_0^{(ab-bx)/a} \left(1-\frac{x}{a}-\frac{y}{b}\right)\left(1-\frac{2x}{a}-\frac{2y}{b}\right)\left(1-\frac{x}{a}-\frac{y}{b}\right)\left(1-\frac{2x}{a}-\frac{2y}{b}\right)dxdy$$

$$= \frac{ab}{60}C$$

$$N_{12} = \rho c\int_0^a \int_0^{(ab-bx)/a} \left(1-\frac{x}{a}-\frac{y}{b}\right)\left(1-\frac{2x}{a}-\frac{2y}{b}\right)\left(\frac{2x^2-ax}{a^2}\right)dxdy$$

$$= -\frac{ab}{360}C = N_{21}$$

$$N_{13} = \rho c\int_0^a \int_0^{(ab-bx)/a} \left(1-\frac{x}{a}-\frac{y}{b}\right)\left(1-\frac{2x}{a}-\frac{2y}{b}\right)\left(\frac{2y^2-by}{b^2}\right)dxdy$$

$$= -\frac{ab}{360}C = N_{31}$$

$$N_{14} = \rho c\int_0^a \int_0^{(ab-bx)/a} \left(1-\frac{x}{a}-\frac{y}{b}\right)\left(1-\frac{2x}{a}-\frac{2y}{b}\right)\frac{4x}{a}\left(1-\frac{x}{a}-\frac{y}{b}\right)dxdy = 0 = N_{41}$$

$$N_{15} = \rho c\int_0^a \int_0^{(ab-bx)/a} \left(1-\frac{x}{a}-\frac{y}{b}\right)\left(1-\frac{2x}{a}-\frac{2y}{b}\right)\frac{4xy}{ab}dxdy$$

$$= -\frac{ab}{90}C = N_{51}$$

$$N_{16} = \rho c\int_0^a \int_0^{(ab-bx)/a} \left(1-\frac{x}{a}-\frac{y}{b}\right)\left(1-\frac{2x}{a}-\frac{2y}{b}\right)\frac{4y}{b}\left(1-\frac{x}{a}-\frac{y}{b}\right)dxdy = 0 = N_{61}$$

$$N_{22} = \rho c\int_0^a \int_0^{(ab-bx)/a} \left(\frac{2x^2-ax}{a^2}\right)\left(\frac{2x^2-ax}{a^2}\right)dxdy$$

$$= \frac{ab}{60} C$$

$$N_{23} = \rho c \int_0^a \int_0^{(ab-bx)/a} \left(\frac{2x^2 - ax}{a^2}\right)\left(\frac{2y^2 - by}{b^2}\right) dxdy$$

$$= -\frac{ab}{360} C = N_{32}$$

$$N_{24} = \rho c \int_0^a \int_0^{(ab-bx)/a} \left(\frac{2x^2 - ax}{a^2}\right)\frac{4x}{a}\left(1 - \frac{x}{a} - \frac{y}{b}\right) dxdy$$

$$= 0 = N_{42}$$

$$N_{25} = \rho c \int_0^a \int_0^{(ab-bx)/a} \left(\frac{2x^2 - ax}{a^2}\right)\frac{4xy}{ab} dxdy$$

$$= 0 = N_{52}$$

$$N_{26} = \rho c \int_0^a \int_0^{(ab-bx)/a} \left(\frac{2x^2 - ax}{a^2}\right)\frac{4y}{b}\left(1 - \frac{x}{a} - \frac{y}{b}\right) dxdy$$

$$= -\frac{ab}{90} C = N_{62}$$

$$N_{33} = \rho c \int_0^a \int_0^{(ab-bx)/a} \left(\frac{2y^2 - bx}{b^2}\right)\left(\frac{2y^2 - by}{b^2}\right) dxdy$$

$$= \frac{ab}{60} C$$

$$N_{34} = \rho c \int_0^a \int_0^{(ab-bx)/a} \left(\frac{2y^2 - bx}{b^2}\right)\frac{4x}{a}\left(1 - \frac{x}{a} - \frac{y}{b}\right) dxdy$$

$$= -\frac{ab}{90} C = N_{43}$$

$$N_{35} = \rho c \int_0^a \int_0^{(ab-bx)/a} \left(\frac{2y^2 - bx}{b^2}\right)\frac{4xy}{ab} dxdy$$

$= 0 = N_{53}$

$$N_{36} = \rho c \int_0^a \int_0^{(ab-bx)/a} \left(\frac{2y^2 - bx}{b^2}\right) \frac{4y}{b} \left(1 - \frac{x}{a} - \frac{y}{b}\right) dxdy$$

$= 0 = N_{63}$

Similarly,

$N_{44} = \frac{4ab}{45} C;\ N_{45} = N_{54} = \frac{2ab}{45} C; N_{46} = N_{64} = \frac{2ab}{45} C;$

$$N_{55} = \frac{4ab}{45} C;\ N_{56} = \ N_{65} = \frac{2ab}{45} C$$

$$N_{66} = \frac{4ab}{45} C.$$

Now evaluating the following integral

$q_j^e = \int_{\Omega^e} f \psi_i^e \, dxdy$, where f is constant.

So,

$$q_1^e = \int_{\Omega^e} f \psi_1^e dxdy = f \int_0^a \int_0^{(ab-bx)/a} \left(1 - \frac{x}{a} - \frac{y}{b}\right) \left(1 - \frac{2x}{a} - \frac{2y}{b}\right) dxdy = 0$$

$$q_2^e = \int_{\Omega^e} f \psi_2^e dxdy = f \int_0^a \int_0^{(ab-bx)/a} \left(\frac{2x^2 - ax}{a^2}\right) dxdy = 0$$

$$q_3^e = \int_{\Omega^e} f \psi_3^e dxdy = f \int_0^a \int_0^{(ab-bx)/a} \left(\frac{2y^2 - by}{b^2}\right) dxdy = 0$$

$$q_4^e = \int_{\Omega^e} f \psi_4^e dxdy = f \int_0^a \int_0^{(ab-bx)/a} \frac{4x}{a} \left(1 - \frac{x}{a} - \frac{y}{b}\right) dxdy = \frac{abf}{6}$$

$$q_5^e = \int_{\Omega^e} f \psi_5^e dxdy = f \int_0^a \int_0^{(ab-bx)/a} \frac{4xy}{ab} dxdy = \frac{abf}{6}$$

$$q_6^e = \int_{\Omega^e} f\psi_6^e dxdy = f\int_0^a \int_0^{(ab-bx)/a} \frac{4y}{b}(1-\frac{x}{a}-\frac{y}{b})dxdy = \frac{abf}{6}$$

The coefficients H_{ij}^e, P_i^e and Q_i^e due to the convective boundary conditions can be computed by evaluating boundary integrals. These coefficients must be computed only for those elements and boundaries that are subject to the convective boundary condition. The boundary integrals are line integrals involving the interpolation function.

The interpolation functions on any given side of quadratic triangular elements are the one dimensional interpolation function. Therefore, the evaluation of integrals is made easy.

$$H_{ij}^e = \oint_{\Gamma^e} \beta\psi_i^e\psi_j^e ds$$

$$H_{11}^e = \oint_{\Gamma^e} \beta\psi_1\ \psi_1\ ds = \beta\{\int_0^a \psi_1\psi_1 dx + \int_a^0 \psi_1\psi_1 dx + \int_0^b \psi_1\psi_1 dy\}$$

$$=0+0+\beta\int_0^b \psi_1\psi_1 dy = \beta\int_0^b \left\{\left(1-\frac{y}{b}\right)\left(1-\frac{2y}{b}\right)\right\}^2 dy = \frac{2\beta b}{15}$$

$$H_{12}^e = \oint_{\Gamma^e} \beta\psi_1\ \psi_2\ ds = 0 = H_{21}^e$$

$$H_{13}^e = \oint_{\Gamma^e} \beta\psi_1\ \psi_3\ ds = \beta\int_0^b \psi_1\psi_3 dy = \beta\int_0^b \left(1-\frac{y}{b}\right)\left(1-\frac{2y}{b}\right)\left(\frac{2y^2-by}{b^2}\right)dy$$

$$=\frac{\beta b}{30} = H_{31}^e$$

$$H_{14}^e = \oint_{\Gamma^e} \beta\psi_1\ \psi_4\ ds = 0 = H_{41}^e$$

$$H_{15}^e = \oint_{\Gamma^e} \beta\psi_1\ \psi_5\ ds = 0 = H_{51}^e$$

$$H_{16}^e = \oint_{\Gamma^e} \beta\psi_1\ \psi_6\ ds = \beta\int_0^b \psi_1\psi_3 dy = \beta\int_0^b \left(1-\frac{y}{b}\right)\left(1-\frac{2y}{b}\right)\frac{4y}{b}(1-\frac{y}{b})dy$$

$=\frac{\beta b}{15} = H_{61}^e$

Similarly,

$H_{22}^e = 0; H_{23}^e = H_{32}^e = 0; H_{24}^e = H_{42}^e = 0; H_{25}^e = H_{52}^e = 0; H_{26}^e = H_{62}^e = 0;$

$H_{33}^e = \frac{2\beta b}{15}; H_{34}^e = H_{43}^e = 0; H_{35}^e = H_{53}^e = 0; H_{36}^e = H_{63}^e = \frac{\beta b}{15};$

$H_{44}^e = 0; H_{45}^e = H_{54}^e = 0; H_{46}^e = H_{64}^e = 0;$

$H_{55}^e = 0; H_{56}^e = H_{65}^e = 0;$

$H_{66}^e = \frac{8\beta b}{15}$

Now evaluate the integral P_i^e and Q_i^e are same only the difference is constant term. Thus, we have

$$P_i^e = \oint_\Gamma \psi_i^e q_n ds = q_n \oint_\Gamma \psi_i^e ds$$

and

$$Q_i^e = \oint_\Gamma \psi_i^e \beta T_\infty ds = \beta T_\infty \oint_\Gamma \psi_i^e ds$$

$$P_1^e = q_n \oint_\Gamma \psi_1^e ds = q_n \oint_\Gamma \left(1 - \frac{x}{a} - \frac{y}{b}\right)\left(1 - \frac{2x}{a} - \frac{2y}{b}\right) ds = \frac{b}{2} q_n$$

$$P_2^e = q_n \oint_\Gamma \psi_2^e ds = q_n \oint_\Gamma \frac{2x^2 - ax}{a^2} ds = 0$$

$$P_3^e = q_n \oint_\Gamma \psi_3^e ds = q_n \oint_\Gamma \frac{2y^2 - by}{b^2} ds = \frac{b}{2} q_n$$

$$P_4^e = q_n \oint_\Gamma \psi_4^e ds = q_n \oint_\Gamma \frac{4x}{a}\left(1 - \frac{x}{a} - \frac{y}{b}\right) ds = 0$$

$$P_5^e = q_n \oint_\Gamma \psi_5^e ds = q_n \oint_\Gamma \frac{4xy}{ab} ds = 0$$

$$P_6^e = q_n \oint_\Gamma \psi_6^e ds = q_n \oint_\Gamma \frac{4y}{b}(1 - \frac{x}{a} - \frac{y}{b}) ds = \frac{b}{2} q_n$$

Similarly,

$$Q_1^e = \oint_\Gamma \psi_1^e \beta T_\infty ds = \beta T_\infty \oint_\Gamma \psi_1^e ds = \frac{b}{2} \beta T_\infty$$

$$Q_2^e = 0;\ Q_3^e = \tfrac{b}{2}\beta T_\infty;\ Q_4^e = 0;\ Q_5^e = 0;\ Q_6^e = \tfrac{b}{2}\beta T_\infty$$

Therefore, the element matrix is

$$[C^e] = \begin{bmatrix} C_{11}^e & C_{12}^e & C_{13}^e & C_{14}^e & C_{15}^e & C_{16}^e \\ C_{21}^e & C_{22}^e & C_{23}^e & C_{24}^e & C_{25}^e & C_{26}^e \\ C_{31}^e & C_{32}^e & C_{33}^e & C_{34}^e & C_{35}^e & C_{36}^e \\ C_{41}^e & C_{42}^e & C_{43}^e & C_{44}^e & C_{45}^e & C_{46}^e \\ C_{51}^e & C_{52}^e & C_{53}^e & C_{54}^e & C_{55}^e & C_{56}^e \\ C_{61}^e & C_{62}^e & C_{63}^e & C_{64}^e & C_{65}^e & C_{66}^e \end{bmatrix} = \frac{ab\rho c}{360} \begin{bmatrix} 6 & -1 & -1 & 0 & -4 & 0 \\ -1 & 6 & -1 & 0 & 0 & -4 \\ -1 & -1 & 6 & -4 & 0 & 0 \\ 0 & 0 & -4 & 32 & 16 & 16 \\ -4 & 0 & 0 & 16 & 32 & 16 \\ 0 & -4 & 0 & 16 & 16 & 32 \end{bmatrix}$$

and

$$K^e = M^e + N^e$$

$$[K^e] = \begin{bmatrix} M_{11}^e & M_{12}^e & M_{13}^e & M_{14}^e & M_{15}^e & M_{16}^e \\ M_{21}^e & M_{22}^e & M_{23}^e & M_{24}^e & M_{25}^e & M_{26}^e \\ M_{31}^e & M_{32}^e & M_{33}^e & M_{34}^e & M_{35}^e & M_{36}^e \\ M_{41}^e & M_{42}^e & M_{43}^e & M_{44}^e & M_{45}^e & M_{46}^e \\ M_{51}^e & M_{52}^e & M_{53}^e & M_{54}^e & M_{55}^e & M_{56}^e \\ M_{61}^e & M_{62}^e & M_{63}^e & M_{64}^e & M_{65}^e & M_{66}^e \end{bmatrix} + \begin{bmatrix} N_{11}^e & N_{12}^e & N_{13}^e & N_{14}^e & N_{15}^e & N_{16}^e \\ N_{21}^e & N_{22}^e & N_{23}^e & N_{24}^e & N_{25}^e & N_{26}^e \\ N_{31}^e & N_{32}^e & N_{33}^e & N_{34}^e & N_{35}^e & N_{36}^e \\ N_{41}^e & N_{42}^e & N_{43}^e & N_{44}^e & N_{45}^e & N_{46}^e \\ N_{51}^e & N_{52}^e & N_{53}^e & N_{54}^e & N_{55}^e & N_{56}^e \\ N_{61}^e & N_{62}^e & N_{63}^e & N_{64}^e & N_{65}^e & N_{66}^e \end{bmatrix}$$

$$= \frac{k}{6ab}\begin{bmatrix} 3(a^2+b^2) & b^2 & a^2 & -4b^2 & 0 & -4a^2 \\ b^2 & 3b^2 & 0 & -4b^2 & 0 & 0 \\ a^2 & 0 & a^2 & 0 & 0 & -4a^2 \\ -4b^2 & -4b^2 & 0 & 8(a^2+b^2) & -8a^2 & 0 \\ 0 & 0 & 0 & -8a^2 & 8(a^2+b^2) & -8b^2 \\ -4a^2 & 0 & -4a^2 & 0 & -8b^2 & 8(a^2+b^2) \end{bmatrix}$$

$$+ \frac{ab\rho c}{360}\begin{bmatrix} 6 & -1 & -1 & 0 & -4 & 0 \\ -1 & 6 & -1 & 0 & 0 & -4 \\ -1 & -1 & 6 & -4 & 0 & 0 \\ 0 & 0 & -4 & 32 & 16 & 16 \\ -4 & 0 & 0 & 16 & 32 & 16 \\ 0 & -4 & 0 & 16 & 16 & 32 \end{bmatrix}$$

$$[H^e] = \begin{bmatrix} H_{11}^e & H_{12}^e & H_{13}^e & H_{14}^e & H_{15}^e & H_{16}^e \\ H_{21}^e & H_{22}^e & H_{23}^e & H_{24}^e & H_{25}^e & H_{26}^e \\ H_{31}^e & H_{32}^e & H_{33}^e & H_{34}^e & H_{35}^e & H_{36}^e \\ H_{41}^e & H_{42}^e & H_{43}^e & H_{44}^e & H_{45}^e & H_{46}^e \\ H_{51}^e & H_{52}^e & H_{53}^e & H_{54}^e & H_{55}^e & H_{56}^e \\ H_{61}^e & H_{62}^e & H_{63}^e & H_{64}^e & H_{65}^e & H_{66}^e \end{bmatrix} = \frac{\beta b}{15}\begin{bmatrix} 2 & 0 & \frac{1}{2} & 0 & 0 & 0 \\ 0 & 0 & 0 & 0 & 0 & 0 \\ \frac{1}{2} & 0 & 2 & 0 & 0 & 1 \\ 0 & 0 & 0 & 0 & 0 & 0 \\ 0 & 0 & 0 & 0 & 0 & 0 \\ 1 & 0 & 1 & 0 & 0 & 8 \end{bmatrix}$$

The conductivity matrix of fig. 3.3 is

$$[K] =$$

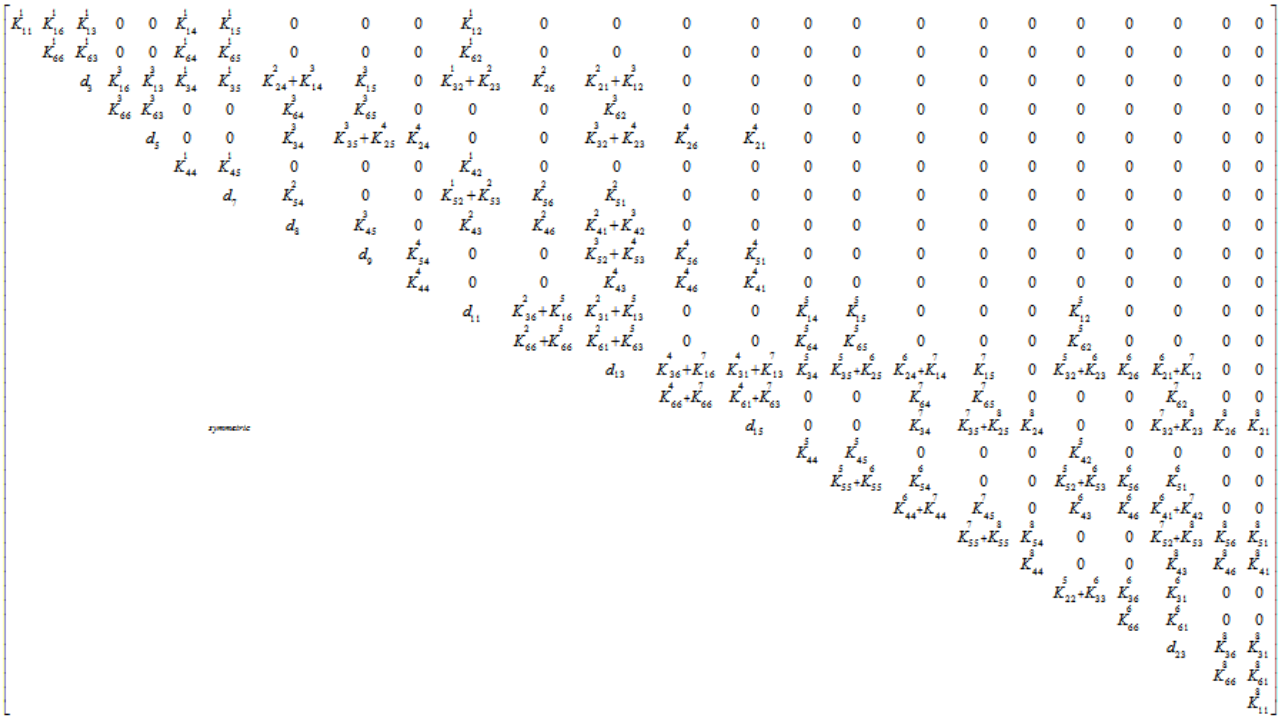

where,

$$d_3 = k_{33}^{1} + k_{22}^{2} + k_{11}^{3},\ d_5 = k_{33}^{3} + k_{22}^{4},\ d_7 = k_{55}^{1} + k_{55}^{2},\ d_8 = k_{44}^{2} + k_{44}^{3},$$

$$d_9 = k_{55}^{3} + k_{55}^{4},\ d_{11} = k_{22}^{1} + k_{33}^{2} + k_{11}^{5},\ d_{13} = k_{11}^{2} + k_{22}^{3} + k_{33}^{4} + k_{33}^{5} + k_{22}^{6} + k_{11}^{7},$$

$$d_{15} = k_{11}^{4} + k_{33}^{7} + k_{22}^{8},\ d_{23} = k_{11}^{6} + k_{22}^{7} + k_{33}^{8}$$

The capacitance matrix is

[C] =

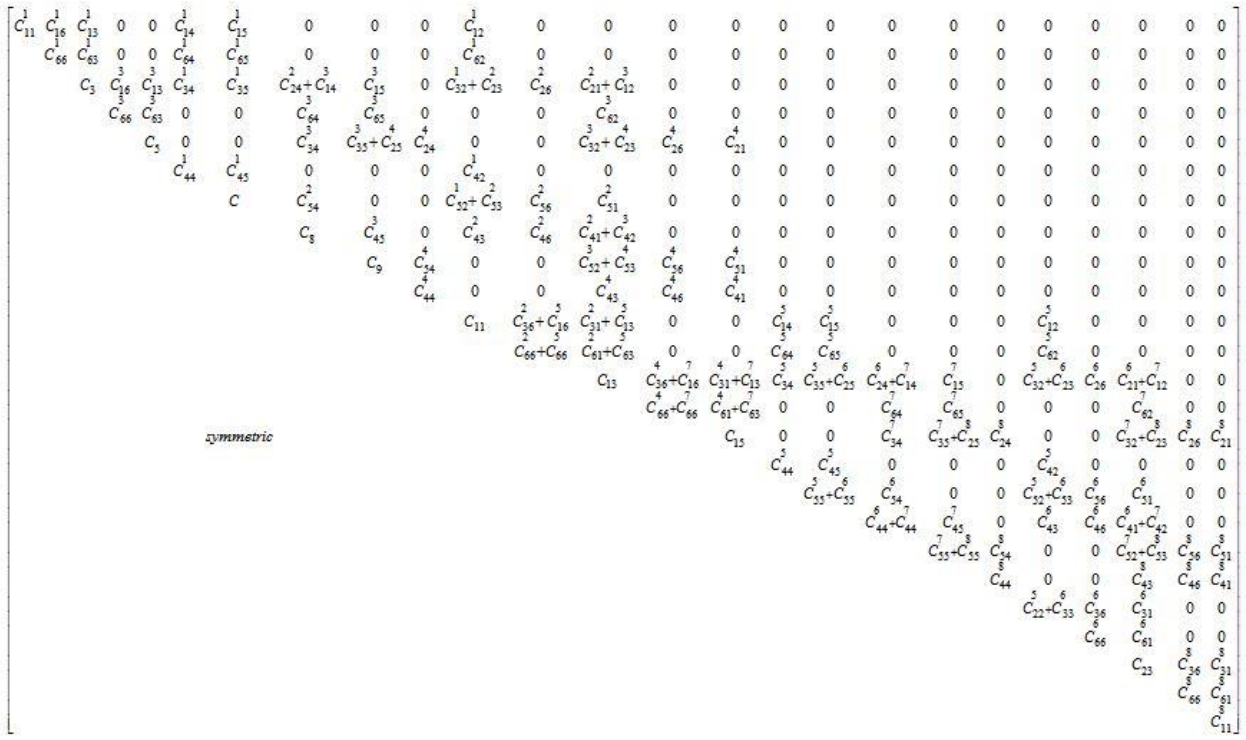

where,

$C_3 = C_{33}^{1} + C_{22}^{2} + C_{11}^{3}$, $C_5 = C_{33}^{3} + C_{22}^{4}$, $C_7 = C_{55}^{1} + C_{55}^{2}$, $C_8 = C_{44}^{2} + C_{44}^{3}$,

$C_9 = C_{55}^{3} + C_{55}^{4}$, $C_{11} = C_{22}^{1} + C_{33}^{2} + C_{11}^{5}$, $C_{13} = C_{11}^{2} + C_{22}^{3} + C_{33}^{4} + C_{33}^{5} + C_{22}^{6} + C_{11}^{7}$,

$C_{15} = C_{11}^{4} + C_{33}^{7} + C_{22}^{8}$, $C_{23} = C_{11}^{6} + C_{22}^{7} + C_{33}^{8}$

3.4 Time Discretization Scheme (Crank-Nicolson Method)

A simple time integration scheme for the Eq.3.13 is derived by assuming that [C] and [K] are constant. In such case, the matrix differential equation can be discretized with respect to time as

$$C\frac{T^{n+1}-T^{n}}{\Delta T}+\alpha KT^{n+1}+(1-\alpha)KT^{n}=q+Q+P \tag{3.6}$$

Where$T^{n+1}$and $T^{n}$are the vectors of unknown nodal values at times $n\Delta T$and$(n+1)\Delta T$ respectively and $\alpha$is the weighting factor, which must be chosen in the interval between 0 and 1. When the value of α is considered 0.5, the process is called the popular Crank-Nicolson method[46]. The discretized Eq.(3.6) can be written as:

$$\left(\frac{C}{\Delta T}+\alpha K\right)T^{n+1}=\left[\frac{C}{\Delta T}-(1-\alpha)K\right]T^{n}+q+Q+P \tag{3.7}$$

The Eq.(3.7) was solved using an iterative procedure. The initial temperature is known and then temperature of the next step can be calculated from the solution of Eq.(3.7) through the Gauss elimination method.

CHAPTER FOUR
HUMAN SKIN MODEL

In this chapter we have discussed our human skin model. Then we clearly explained boundary conditions of this model. We have developed computer code (Using programming Language C) to compute this model. Our result obtained from our finite element code will be compared with analytical solution available in the literature. Computer code developed to solve two dimensional problems will be compared with COMSOL-Multiphysics5.0. Finally, we have explained our numerical results in steady state case and time dependent case.

4.1 Human Skin Model

The human skin is usually modeled as a three layered region in the coordinate system XOY. Three distinct regions are considered, explicitly the epidermis (top layer), dermis (middle layer) and subcutaneous fat (bottom layer) respectively. On the epidermis surface heating disk at constant temperature is applied. This is shown in Fig. 1.

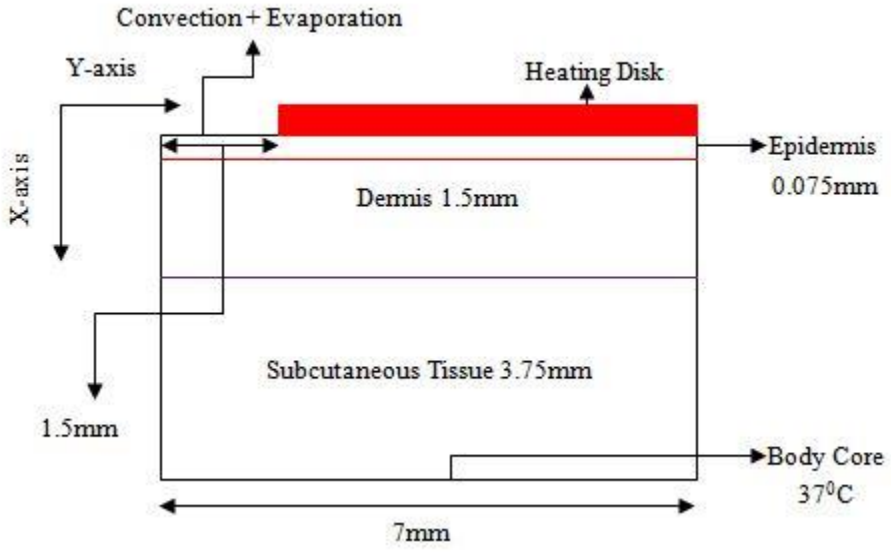

Figure 1.1The human skin model

In biomechanical engineering, the human skin tissue is usually modeled as a three-layer material structure including the epidermis, the dermis, and the subcutaneous fat layer. In a three-layer biomechanical model in this study shown in Fig. 4.1, each layer is supposed to be

ideally homogeneous, within which the thermal conductivity ,blood perfusion, and heat capacity are assumed to be constant, and layers are considered to be perfectly linked each other to permit a continuous flow of heat flux across interfaces. Our finite element mesh (quadratic triangular elements) contains 1988 elements and 4147 nodes. 28 elements are considered in the epidermis area, 560 elements in the dermis region and 1400 elements in the subcutaneous fat region. In case of triangular element finite element mesh contain same number of elements with 1080 nodes. In our model, we can not see the significant difference of computed results by using quadratic triangular and triangular elements. This may be our model is very small. During computation temperature boundary condition will be applied at the body core and heat flux and convection boundary condition will be applied on the skin surface depending upon the conditions.

In the case of determining skin burn, we divided human skin into three layers named as epidermis, dermis, and subcutaneous tissue. Each layer has distinct thermal properties. The properties of skin used in this study are as below:

Table 1.1values of parameters used in this study

Parameter	Value	Parameter	Value
Thermal conductivity: Epidermis Dermis Subcutaneous tissue	 0.21 W/m^2 0.37 W/m^2 0.16 W/m^2	Density Epidermis Dermis Subcutaneous tissue	 1200 kg/m^3 1000 kg/m^3 1000 kg/m^3
Blood Perfusion: Epidermis Dermis Subcutaneous tissue	 0 ml/s/ml 0.00125 ml/s/ml 0.00125 ml/s/ml	Specific heat Epidermis Dermis Subcutaneous tissue	 3598 $Jkg^{-1}{}^0C^{-1}$ 3222 $Jkg^{-1}{}^0C^{-1}$ 2760 $Jkg^{-1}{}^0C^{-1}$
Density of Blood	1100 kg/m^3	Pre exponential factor (P)	3×10^{98}[1/s]
Specific heat of blood	3300 $Jkg^{-10}C^{-1}$	Activation Energy (ΔE)	$6.3\times10^8 Jkg^{-1}k^{-1}$
Evaporation Rate	10 W/m^2	Molar Gas Constant (R)	$8.314\times10^3 JKmol^{-1}K^{-1}$
Temperature of the artery	34 °C	Heating Time	30s
Heat convection coefficient	7 W/m^2 °C		
Environmental temperature	25 °C		

4.2 The Boundary Conditions

Boundary conditions are necessary in order for a solution of the governing Eqs. (1.1) to be obtained. We specify boundary conditions on the boundaries Γ_1- $\Gamma_5$in Fig 4.2 based on the anatomical and physiological observations of actual human skin. Boundary Γ_1 denotes the bottom surface of the human skin, we consider that the temperature is same as the body core which is not affected by the hot disk placed on the surface of the human skin.

Hence we may write

$$T = T_b \text{ at boundary } \Gamma_3$$

where$T_b$is the body core temperature. Boundaries Γ_4 and $\Gamma_5$are assumed to be thermally insulated. Consequently, we may write

$$-k\frac{\partial T}{\partial x} = 0 \text{ at boundaries } \Gamma_4 \text{ and } \Gamma_5$$

The part of the epidermal surface is directly exposed to the environmental fluid, therefore the heat exchange occurs between the environmental fluid and skin via convection and radiation. This is because in biological tissues, the effect of radiation from the surrounding is very small in contrast to convection, thus radiation is neglected. Also, the cooling of the human skin by the evaporation of sweat should be considered since the heat loss due to evaporation has been found to contribute approximately 15% of the total heat loss from the skin surface[3,43]. Thus, we have,

$$-k\frac{\partial T}{\partial x} = h_b(T - T_0) + E \quad \text{at boundary } \Gamma_1$$

where E is the heat loss due to sweat evaporation on the skin surface, and h_b and T_0 are respectively the ambient convection coefficient and temperature.

Finally, on the boundary where the heating disk is applied, the temperature is assumed to be equal to the temperature of heating disk T_d, i.e

$$T = T_d \quad \text{at boundary } \Gamma_2$$

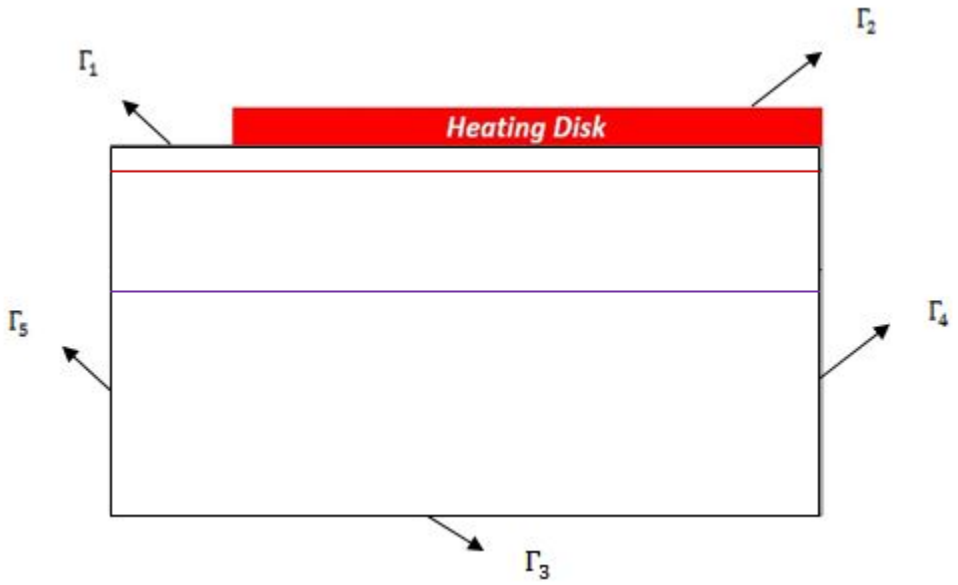

Figure 1.2 Peripheral boundaries where the boundary conditions are specified for FEM.

4.3 Development of Computer Code

A computer code is developed using computer language C for computing results of two dimensional problems. This computer code can handle linear triangular elements and quadratic triangular elements. This computer code may handle any kind of inhomogeneity of thermal properties. This code can impose any type of boundary condition as discussed in chapter two at any boundary.

4.4 Code Verification

As the analytical solution of Pennes bio-heat equation in two dimension is very difficult to obtain. That is why, to test our two dimensional computer code we developed similar model of the problem described in section 3.1 in COMSOL-Multiphysics which is a general-purpose software platform, based on advanced numerical methods, for modeling and simulating

physics-based problems. And we compare our result with the result obtained from COMSOL-Multiphysics. Fig 4.3 and Fig 4.4 show that our result is very close to the COMSOL-Multiphysics result. So the computer code and the solution procedure are reliable for further study. Typical tissue properties used in this section are given in Table 4.1. We also compare our computed result with the one dimensional analytical solution that found in literature[17]. In Fig. 4.5 noticed that our computed result exactly same as the analytical result.

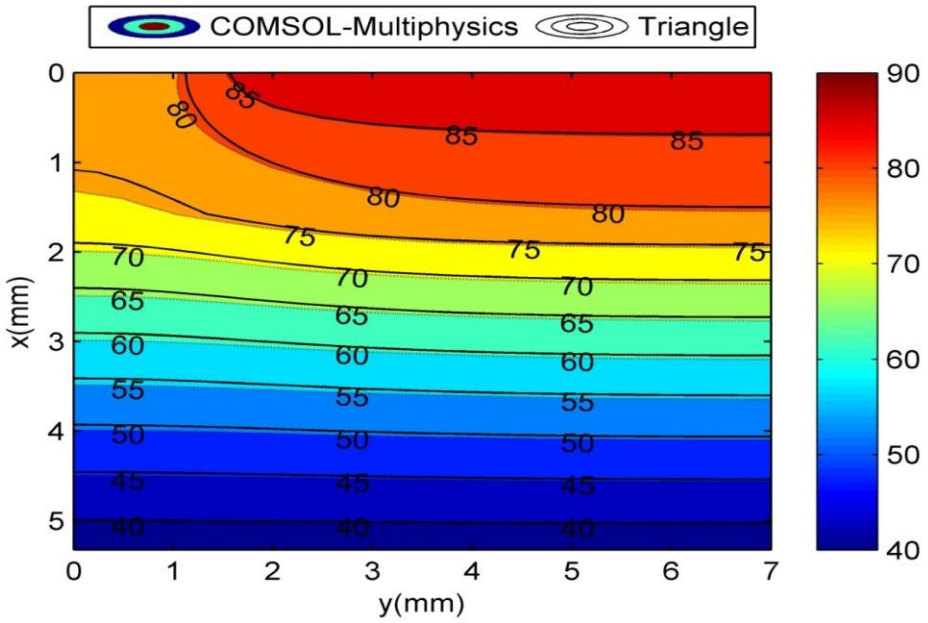

Figure 1.3 Comparison results of triangle and COMSOL- Multiphysics.

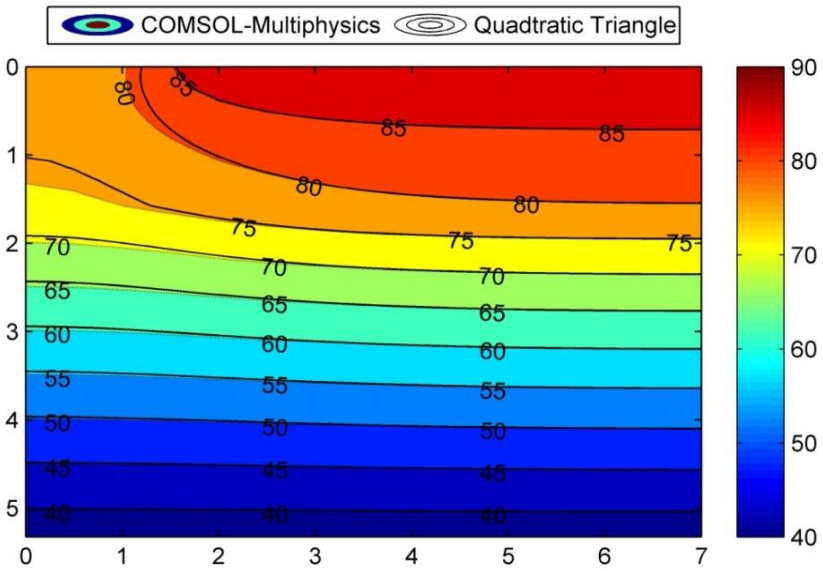

Figure 1.4 Comparison results of quadratic triangle and COMSOL-Multiphysics.

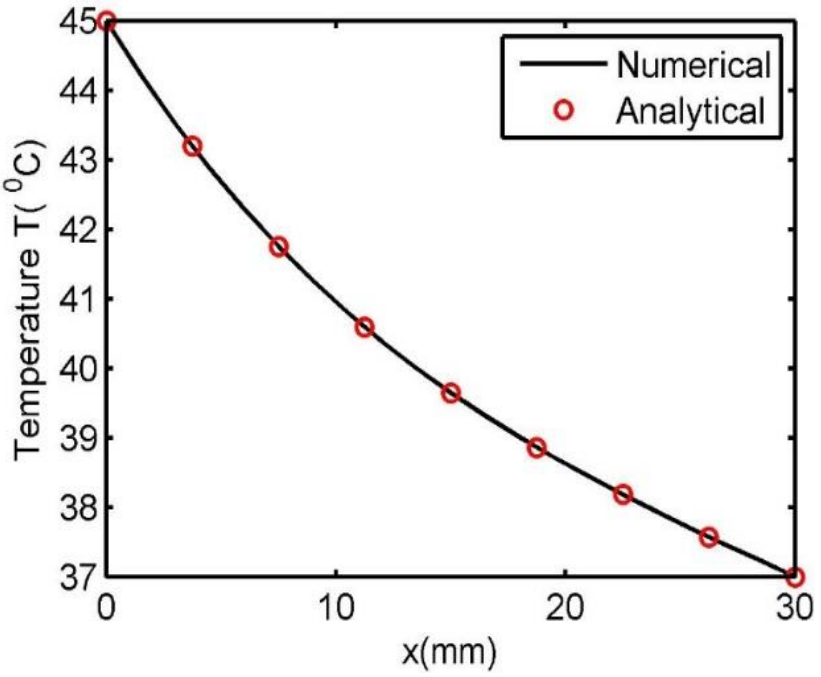

Figure 1.5 Comparison with analytical result.

4.5 Steady State Case

The temperature distribution inside the solution domain was investigated with different values of parameters including the thermal conductivity of epidermis, dermis and subcutaneous fat, heating disk temperature, ambient temperature, ambient convection coefficient, evaporation rate of sweat, and blood perfusion rate to investigate the seriousness of burn. The purpose of such analysis, also called sensitivity analysis, is to identify the effects of individual or a combination of parameters on the temperature distribution within the skin tissue during outer burn process.

Fig. 4.6 represents the temperature profile inside the human skin model obtained using values of parameters tabulated in table 4.1. The highest temperature (depicted in red) is noticed at the surface where the heating disc is applied. However, the lowest temperature takes place at the bottom of the skin (depicted in blue), which is same at the body core temperature of 37^0C. The solid lines in Fig. 4.6 show the isotherms inside the human skin. Temperature at the surface which is exposed to the ambient of the epidermis is found to be approximately 75^0C. This may be due to the exposure of the human skin to the environment. As the skin comes in contact with the heating disc, heat flows from the heating disc into the skin. The excess heat is transferred to the environment via convection and evaporation from the surface of the epidermis. Blood perfusion inside the dermis also serves as a medium to diffuse away the additional heat from the skin tissue.

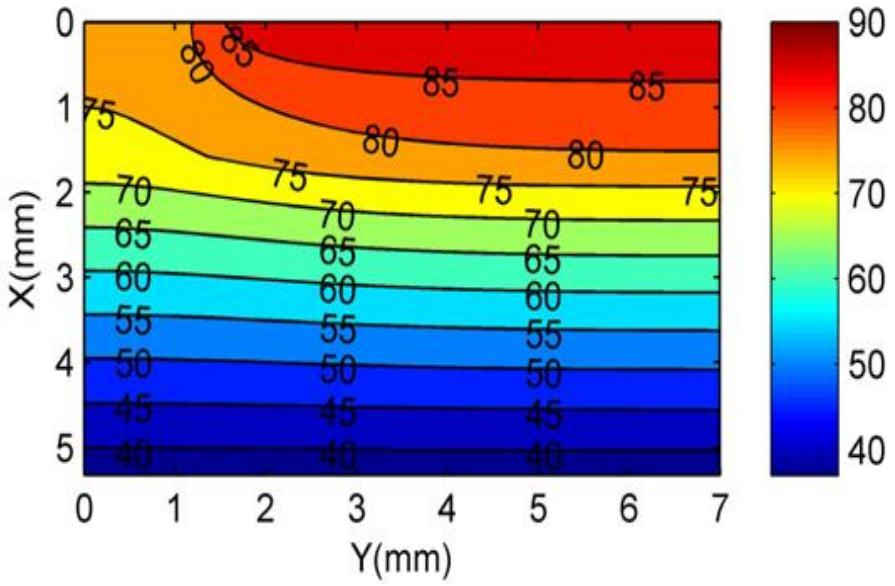

Figure 1.6 Steady state temperature distribution in human skin.

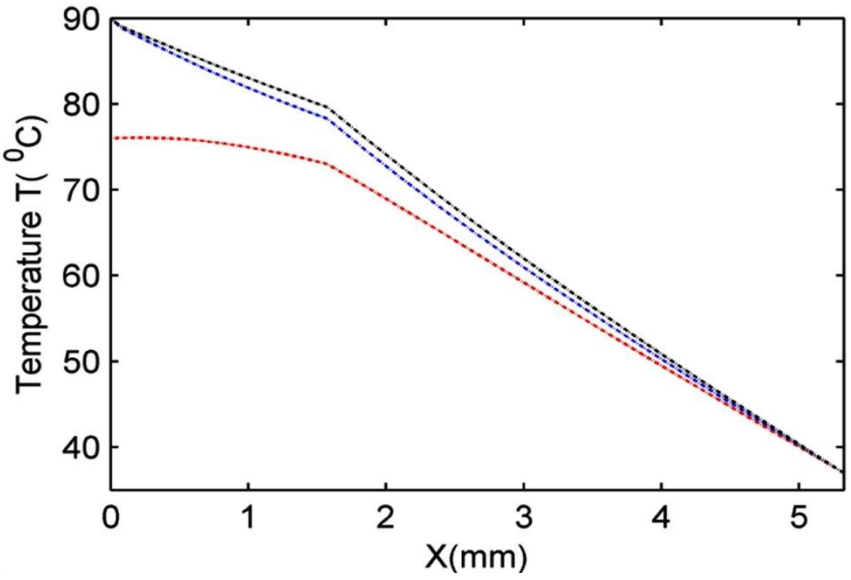

Figure 1.7 Temperature distributions along x-axis. Red line, y = 0 mm; Blue line, y = 3 mm; and Black line, y = 7 mm.

Fig. 4.7 sketch the temperature profile along the *x*-axis at *y* = 0 mm, *y* = 3 mm and y = 7 mm. These values of *y* are selected to provide a more absolute visualization of the temperature distribution inside the human skin. The temperature of the skin seems to increase uniformly inside the region occupied by the subcutaneous fat. Inside the dermis, a rapid increase at *y* = 3mm and y = 7mm is observed. This may be due to the fact this region is very close to the

heating disk. The rate of temperature rise falls at y = 0mm because the heat loss from epidermis to ambient.

4.5.1 Sensitivity analysis

In this section, a sensitivity analysis is accomplished which is very important to examine how changes in the various parameters of the human skin during burns may affect the skin temperature distribution. We also categorize the parameter(s) that have dominant effects on the human skin. Since the seriousness of burns and the thermal injury inflicted on the skin are dependent on the temperature increase, it may be advantageous if the clinical significance of each parameter is analyzed.

In this analysis, eight parameters are considered, specifically the thermal conductivity of the epidermis, dermis and subcutaneous fat, disc temperature, blood perfusion rate, ambient convection coefficient, ambient temperature and evaporation rate of the skin surface. To investigate how changes in each of these parameters may affect the skin temperature distribution, values of these parameters are varied by a certain amount from the control level (table 1). For investigation of each parameter, values of other parameters keeping fixed of its control. Two different values are assumed that one is higher and another is lower than control value. Observations are made along the *x*-axis at y = 0mm, y = 3mm and *y* = 7mm. Sketch these figure in order to obtain a more complete visualization of how the changes in each parameter affect the temperature distribution inside the skin.

4.5.1.1 Effect of epidermis thermal conductivity

The control value of the epidermis thermal conductivity is selected to be $0.21 Wm^{-1} K^{-1}$. In practical situation, thermal conductivity varies for individual and various part of human body. For this reason considered two values to be 0.105 and 0.42 $Wm^{-1}K^{-1}$ which is lower and higher than the control value. The effect all of these values are investigated.

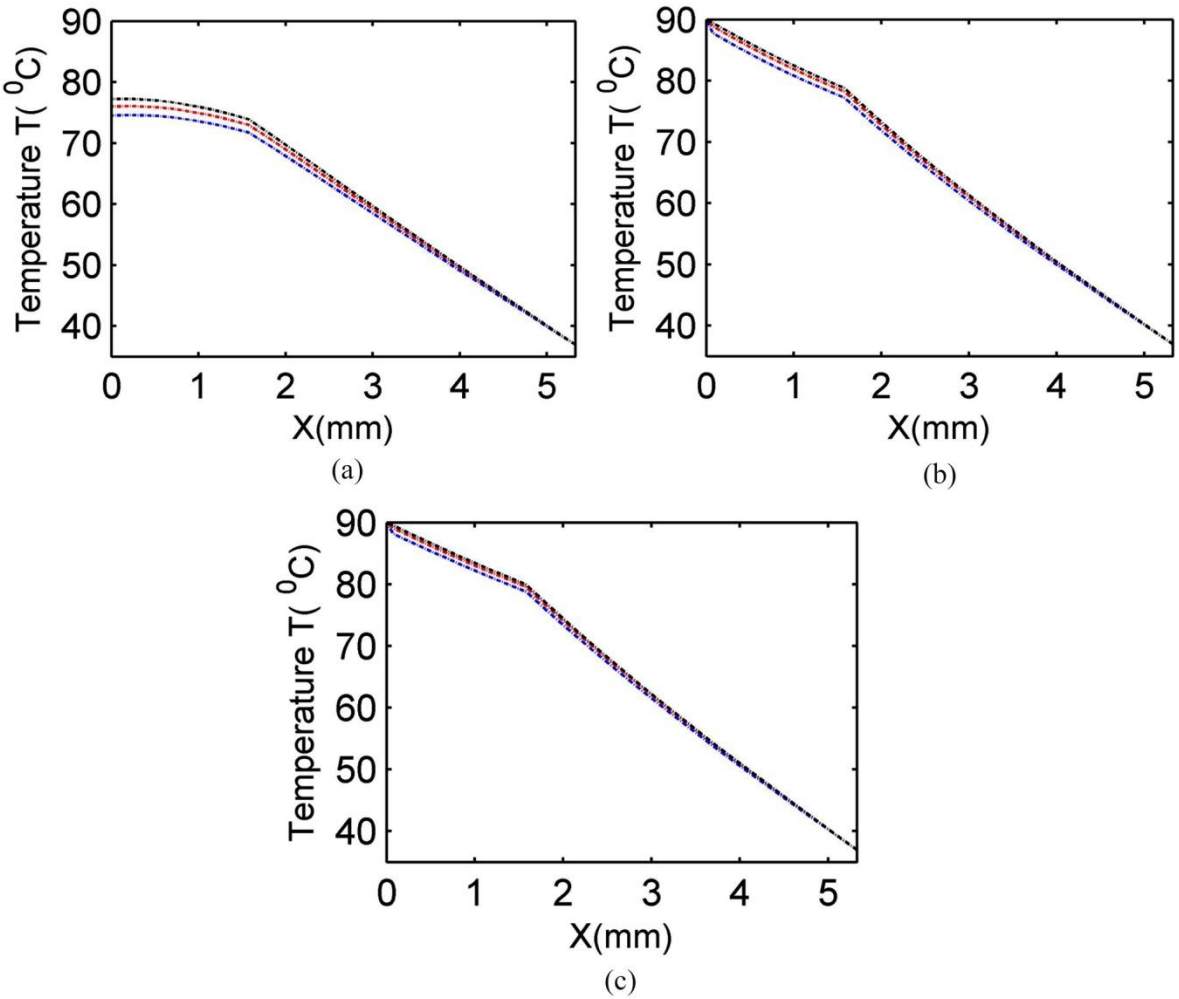

Figure 1.8 Effect of Epidermis thermal conductivity. (a) y = 0mm,(b) y = 3.5mm and (c) y = 7mm.Red lines, *k* = 0.21; Black lines, *k* = 0.42; and Blue lines, *k* = 0.105.

Fig. 4.8 demonstrates the results of investigation. Variation of the epidermis thermal conductivity seems to have a very small effect on the temperature distribution inside the human skin. This may be due to the very thin structure of the epidermis, which causes any changes in the thermal conductivity to have an insignificant impact on the thermal response of the entire system. The results obtained here imply that in examining the damage to the skin, the epidermis will most likely suffer the worst injury since the heat from the burn source is transferred directly across this region.

4.5.1.2 Effect of dermis thermal conductivity

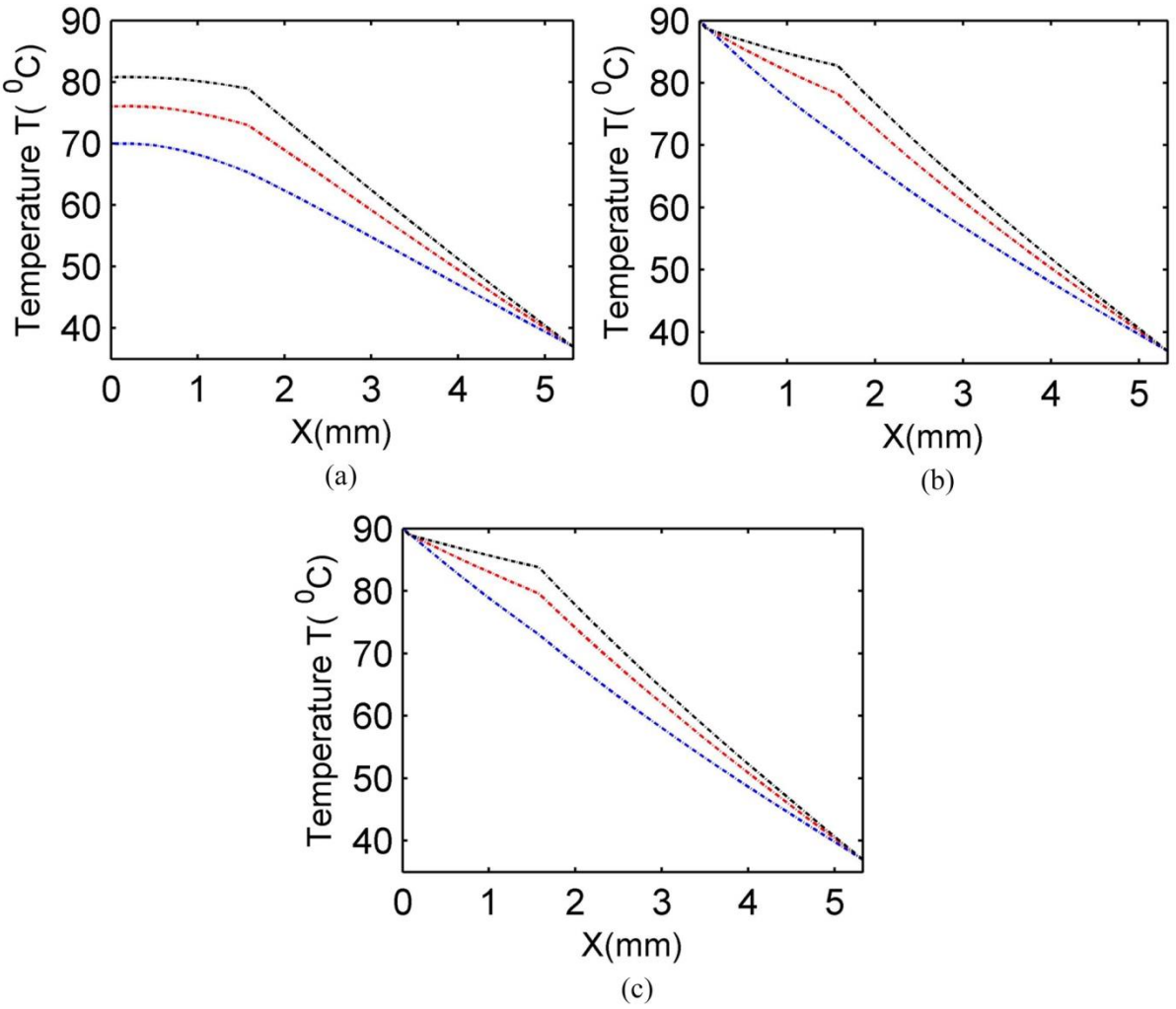

Figure 1.9 Effect of dermis thermal conductivity. (a) y =0mm,(b) y =3.5mm and (c) y = 7mm.Red lines, *k* = 0.37; Black lines, *k* = 0.74; and Blue lines, *k* = 0.185.

Using the same argument as that presented for the epidermis thermal conductivity, values of 50 and 200 per cent of the control are investigated for the dermis thermal conductivity. These values correspond to 0.185 and 0.74$Wm^{-1}K^{-1}$, respectively. The results obtained are presented in Fig. 4.9. It can be noticed that the temperature inside the dermis is higher whose thermal conductivity is higher. Variation of the dermis thermal conductivity has a less important effect on the temperature distribution inside the skin.

4.5.1.3 Effect of subcutaneous fat thermal conductivity

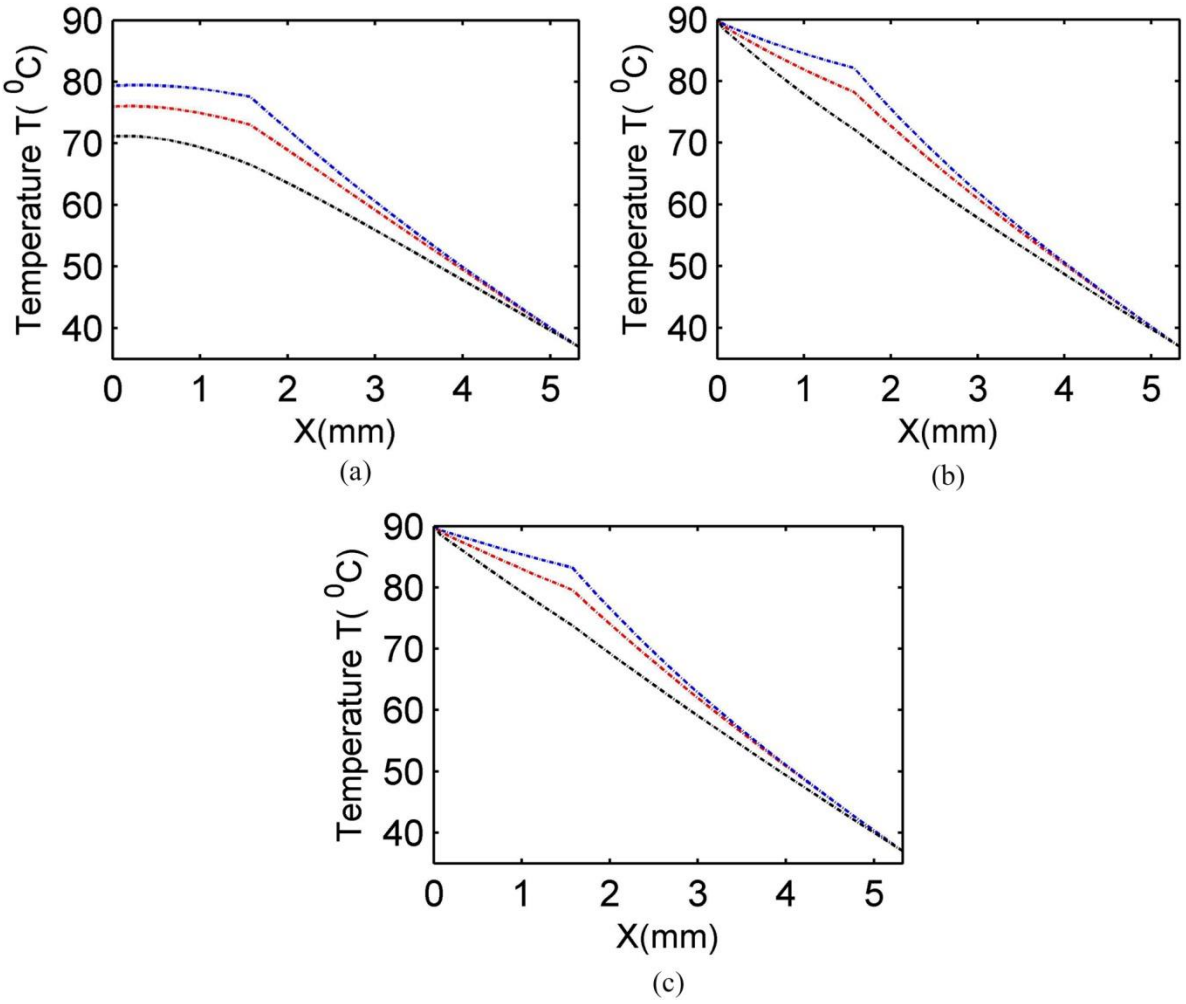

Figure 1.10 Effect of subcutaneous fat thermal conductivity. (a) y = 0mm,(b) y = 3.5mm and (c) y = 7mm. Red lines, *k* = 0.16; Black lines, *k* = 0.32; and Blue lines, *k* = 0.08.

Values of the subcutaneous fat thermal conductivity corresponding to 50 and 200 per cent of the control are given by 0.08 and 0.32Wm^{-1} K^{-1}, respectively. The obtained numerical results are illustrated in Fig. 4.10. From Fig.4.10, an increase in the subcutaneous fat thermal conductivity is found to produce a slight decrease in the temperature at the interface between the subcutaneous fat and the dermis layer (y =1.5mm). In other words, a larger fat thermal

conductivity produces a cooler tissue temperature. A higher thermal conductivity allows the skin tissue to cool down faster, thus resulting in less damage to the tissue.

4.5.1.4 Effect of disk temperature

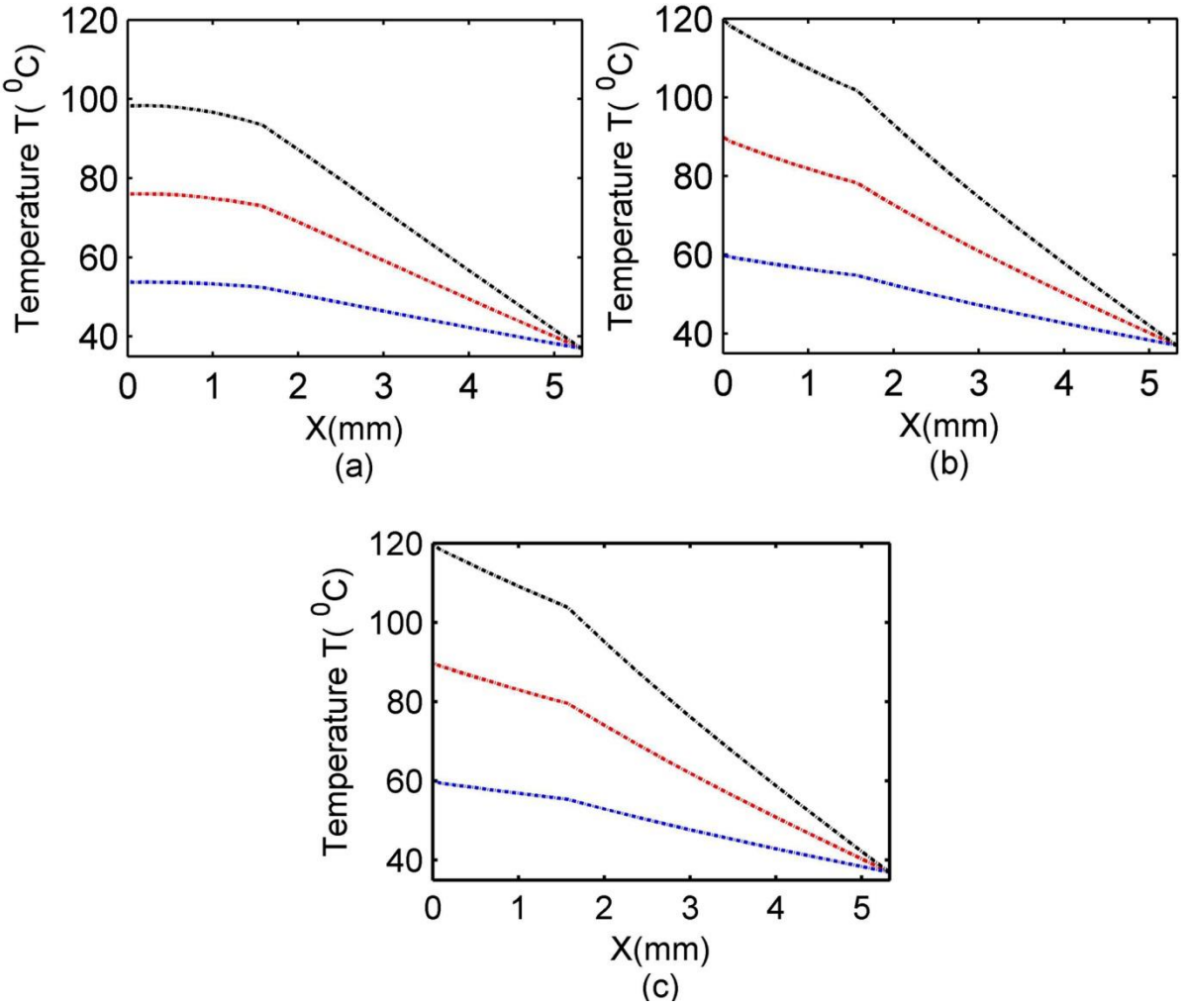

Figure 1.11 Effect of disk temperature. (a) y= 0 mm,(b) y = 3mm and (c) y = 7mm. Red lines, T_d= 90°C; Black lines,T_d = 120°C; and Blue lines,T_d = 60°C.

Two different values are chosen to be 60°C and 120°C respectively which is lower and greater than the control value for investigating the effect of the disk temperature on the isotherm inside the human skin under the constant heating burn. The results are illustrated in Fig. 4.11. This figure reveals that the skin temperature at y = 3mm and 7mm show a small thermal variation

when compared with the variations at y = 0mm. This is not astonishing because the source of heat lies in the regions along y = 3mm and 7mm while at y = 0mm, cooling takes place at the surface of the skin that is exposed to ambient. We notice that the lowest temperature occurs at the body core region of the skin tissue and the hottest surface is a surface where the heating disk is applied. The lines represent higher temperature whose disk temperature is higher. It also seems that the temperature at the convection surface has a higher value than the core temperature 37^0C, since heat supply from the heating disk is basically transferred to the environment via convection and sweat evaporation. Further, there is no observable change of temperature in the epidermis layer because it is too thin (only 0.075 mm).

4.5.1.5 Effect of blood perfusion rate

To examine the effect of blood perfusion rate inside the skin during the temperature distribution, the values of perfusion rate are chosen to be 0.0005 ml/s/ml, 0.00125 ml/s/ml , and 0.024 ml/s/ml, where 0.00125 ml/s/ml is assumed to be a control value and other two are considered lower and higher values of control. These three different values are selected with a view to understand the role of blood flow in the thermoregulation of the biological tissue when it suffers burns. The effect of blood perfusion rate inside the skin during the temperature distribution are illustrate in Fig. 4.12. It has been seen that higher blood perfusion rate reduce the temperature inside the skin. When the tissue temperature is increased, the immediate effect for the body to cause the blood vessels to expand and then increase the blood flow to decline the heat accumulated in the body, resulting in less damage of the tissue. Thus, the overall tissue temperature falls when the blood perfusion rate increases. The results demonstrated in this figure recommend that to decrease damage to the skin due to burn, increasing blood flow through the tissue may help to transfer away the excess heat.

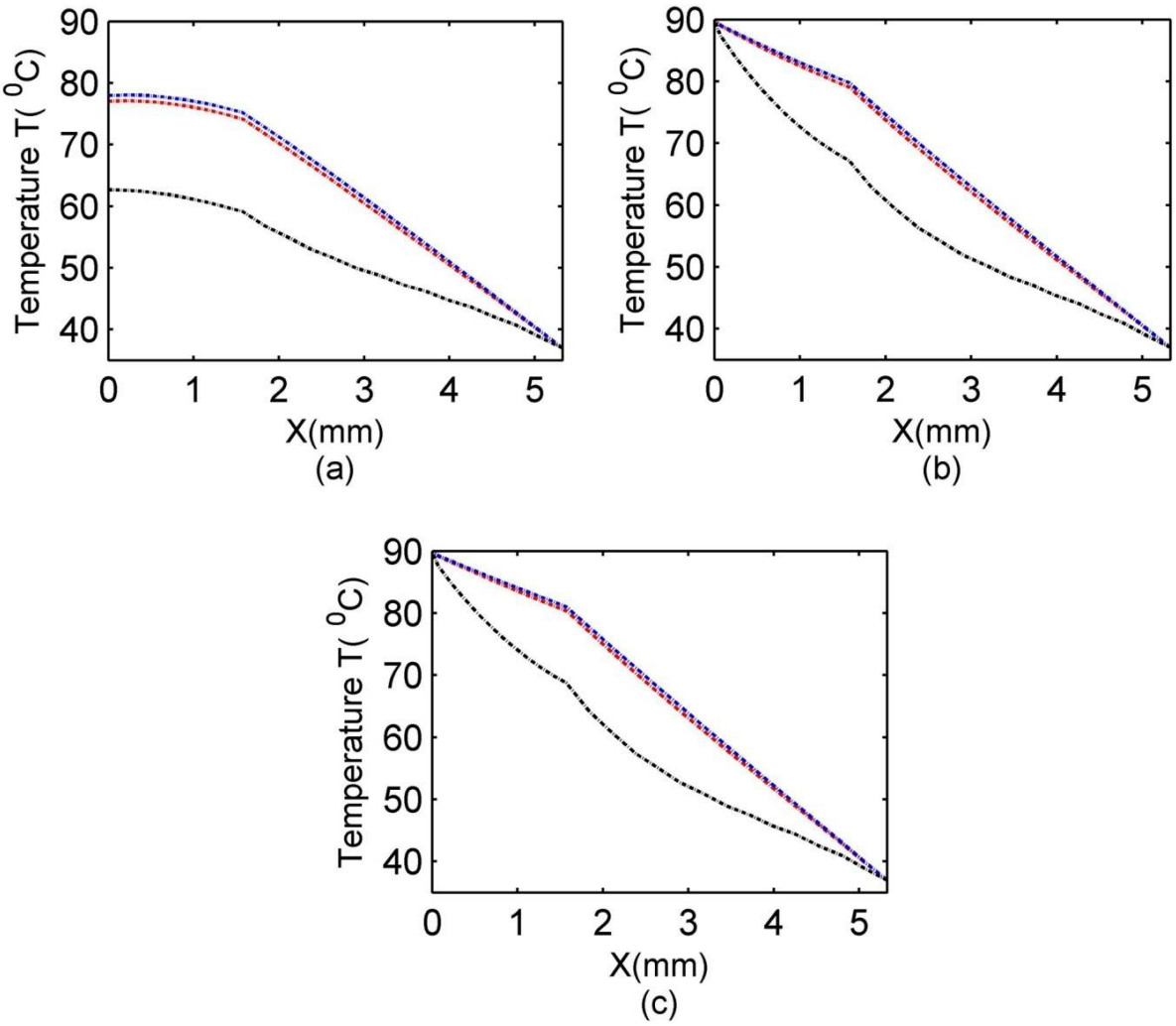

Figure 1.12 Effect of blood perfusion rate. (a) y = 0mm,(b) y = 3mm and(c) y = 7mm. Red lines, w_b= 0.00125 ml/s/ml; Black lines,w_b = 0.024 ml/s/ml; and Blue lines,w_b = 0.0005 ml/s/ml.

4.5.1.6 Effect of ambient heat transfer coefficient

The effect of ambient convection coefficient during burn inside the human skin is investigated. The control value for the ambient convection coefficient is 7Wm^{-2} K^{-1}. This value implies a natural convection condition at the skin surface. We shall consider values of 25Wm^{-2} K^{-1} which is the onset from natural convection to forced convection and 250Wm^{-2} K^{-1} to simulate forced convection.

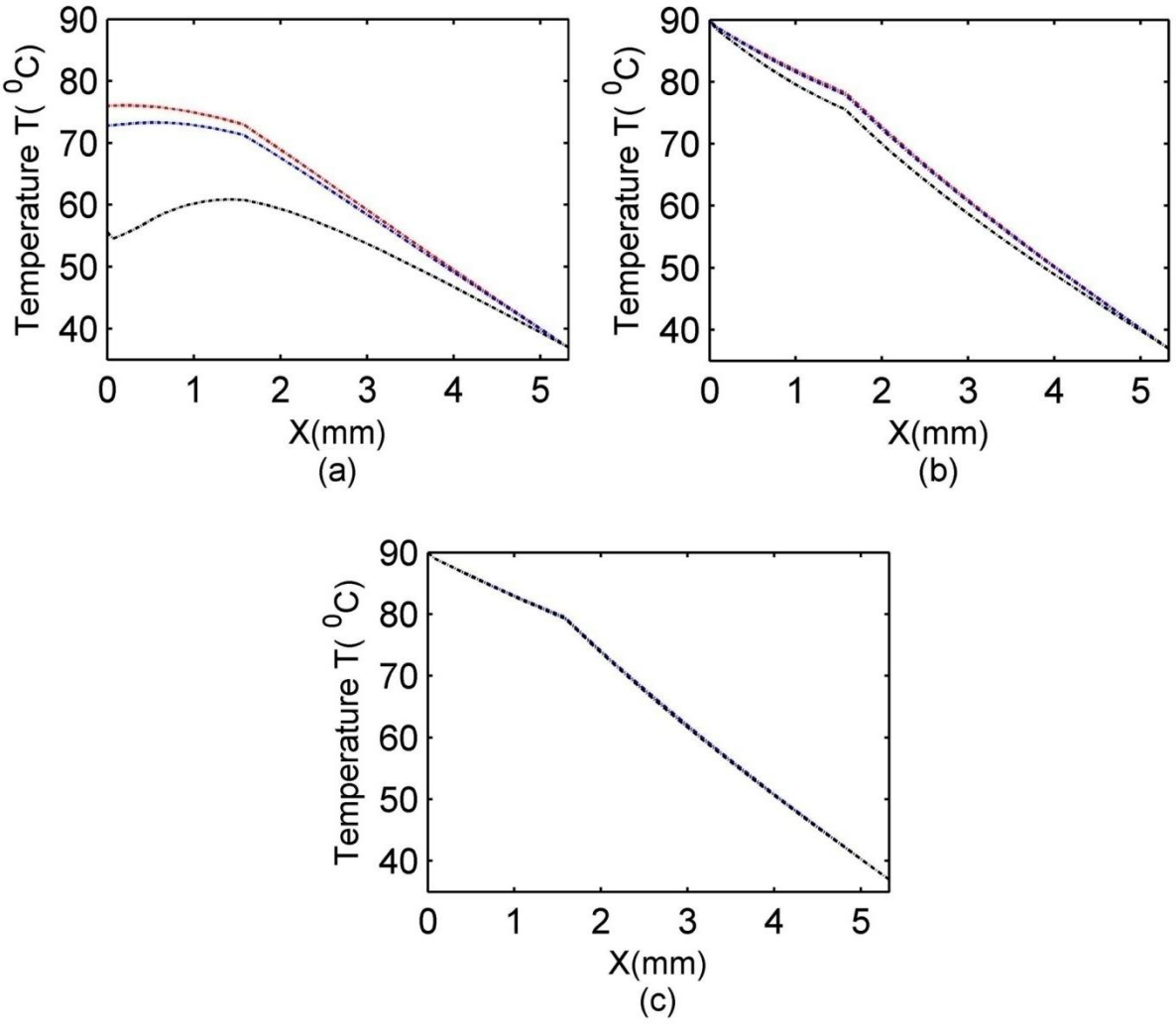

Figure 1.13 Effect of ambient convection coefficient. (a) y = 0mm,(b) y = 3mm and(c) y = 7mm. Red lines, h = 7Wm^{-2} K^{-1}; Black lines,h =250Wm^{-2} K^{-1}; and Blue lines,h =25Wm^{-2} K^{-1}.

The temperature of ambient is assumed to be 25^{0}C. Results are demonstrated in Fig. 4.13. This figure shows that the convection coefficient has little effect on temperature distribution at y = 7mm inside the skin. However, we noticed significant effect on temperature distribution at y = 0mm the convection surface of the skin. Where, the temperature decrease significantly along with convection coefficient increases. In clinical practice, the results suggested that the thermal damage can be reduced by imposing forced convection at the skin surface.

4.5.1.7 Effect of ambient temperature

We assumed 25^0C of the ambient temperature as a control value. To analyzed the effect of ambient temperature inside the skin during burn. Two values 16^0Cand 40^0C are considered which is lower and higher ambient temperature than the control value. The results are presented in Fig. 4.14 shows that the effect of different ambient temperature on the temperature distribution inside the skin is negligible. This suggests that lowering the ambient temperature may not be good idea to avoid the risk of thermal damage on the skin of individuals who have suffered burns.

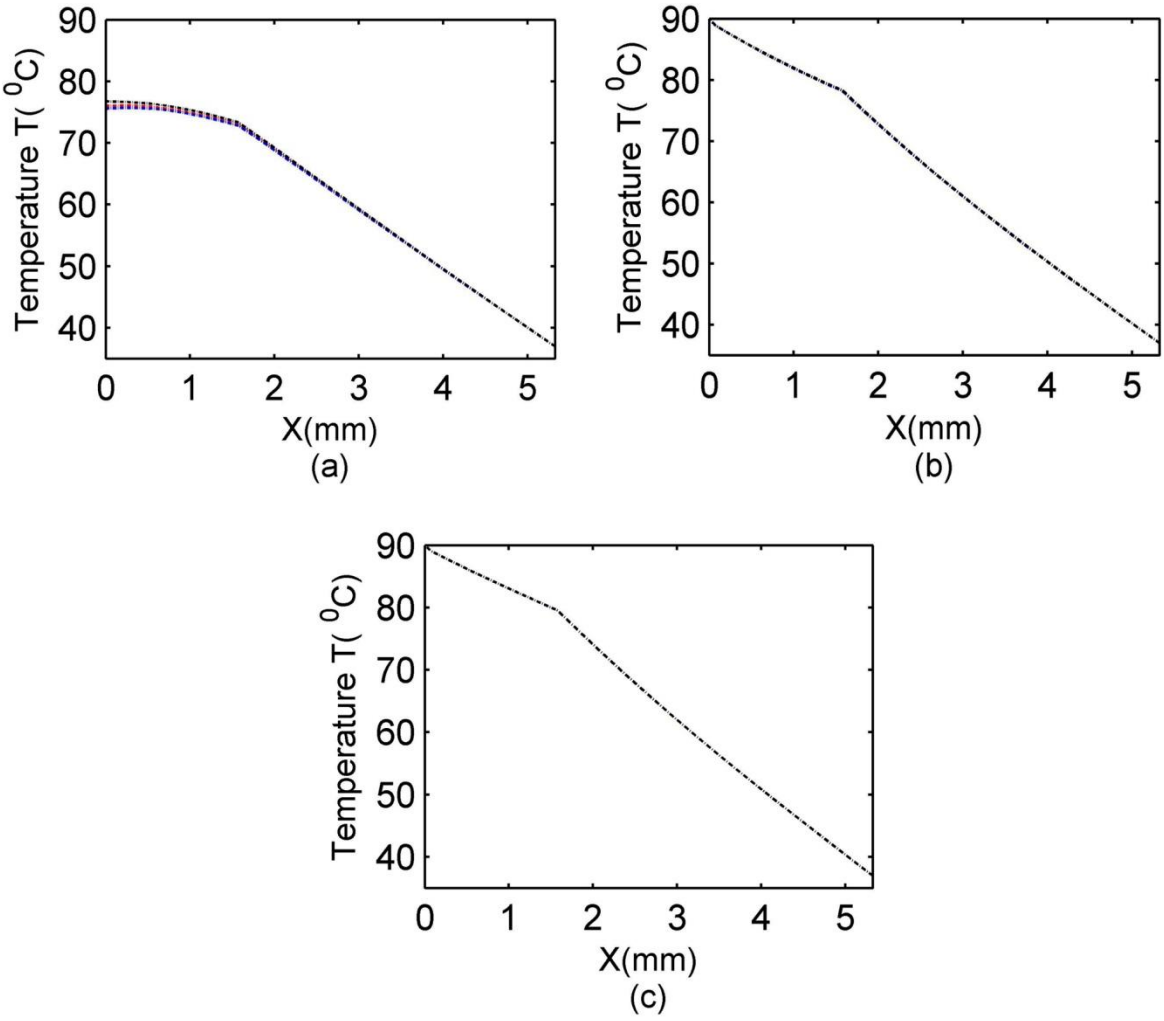

Figure 1.14 Effect of ambient temperature. (a) y = 0mm,(b) y = 3mm and(c) y = 7mm. Red lines, T_0= 25^0C; Black lines,$T_0 = 40^0$C; and Blue lines $T_0 = 16^0$C.

4.5.1.8 Effect of skin evaporation rate

The control value for sweat evaporation rate is taken to be $10W/m^2$. The values of evaporation rate represent the heat loss owing to the evaporation of sweat from the human skin. To examine how lower and higher values may change the temperature distribution inside the skin, values of 0 and 15Wm−2 are selected. Results are displayed in Fig. 4.15. The various values of the evaporation rate show almost no effect on the temperature distribution inside the human skin. This is only to be expected since heat loss owing to evaporation contributes only approximately 15 percent of the total heat loss from the skin surface [47]. Perhaps a larger evaporation rate may have some observable effects.

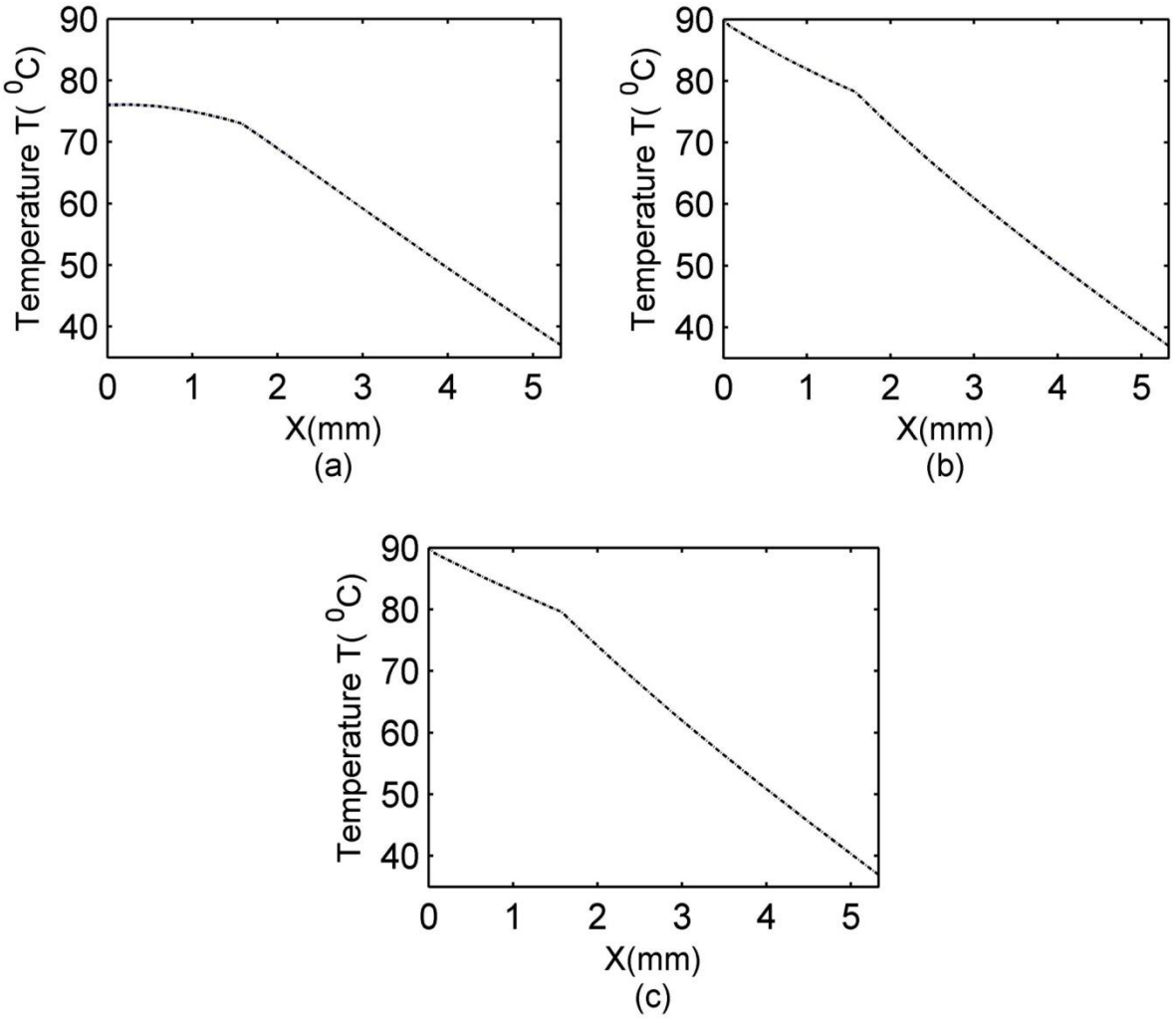

Figure 1.15 Effect of evaporation rate. (a) y = 0mm,(b) y = 3mm and(c) y = 7mm. Red lines, E =10Wm^{-2}, Black Lines, E = 15Wm^{-2}and Blue lines, E = 0Wm^{-2}.

4.6 Time dependent Case

A two-dimensional finite element program has been developed to solve the equation (3.12) and simulate the transient temperature field produced in the skin. The finite element method[48,49] is a modeling technique which has several benefits over the more standard finite difference methods for solving heat transfer problems in biomedical applications. Although the finite element method has been used for many years in stress analysis problems, it has recently been applied for modeling of biomedical heat transfer[50-53]. In the finite element method, the region of interest is divided into small regions, or elements. These regions are usually three or four-sided shapes which may have curved boundaries. Different material properties may be assigned to each element. The differential equation (3.12) is solved in an average or integrated sense over each element and the boundary conditions are satisfied in an averaged sense over each element edge which lies on the boundary. The finite element method can accommodate prescribed temperature, heat flux, or convective-type boundary conditions without a loss of accuracy near the boundary, and it automatically imposes continuity of temperature fields and heat flux at all element interfaces. Hence, temperatures and fluxes are continuous at intermaterial boundaries. A Crank-Nickolson time stepping method is used, and it is well known that the numerical technique used here is second order accurate in both time and space[54].

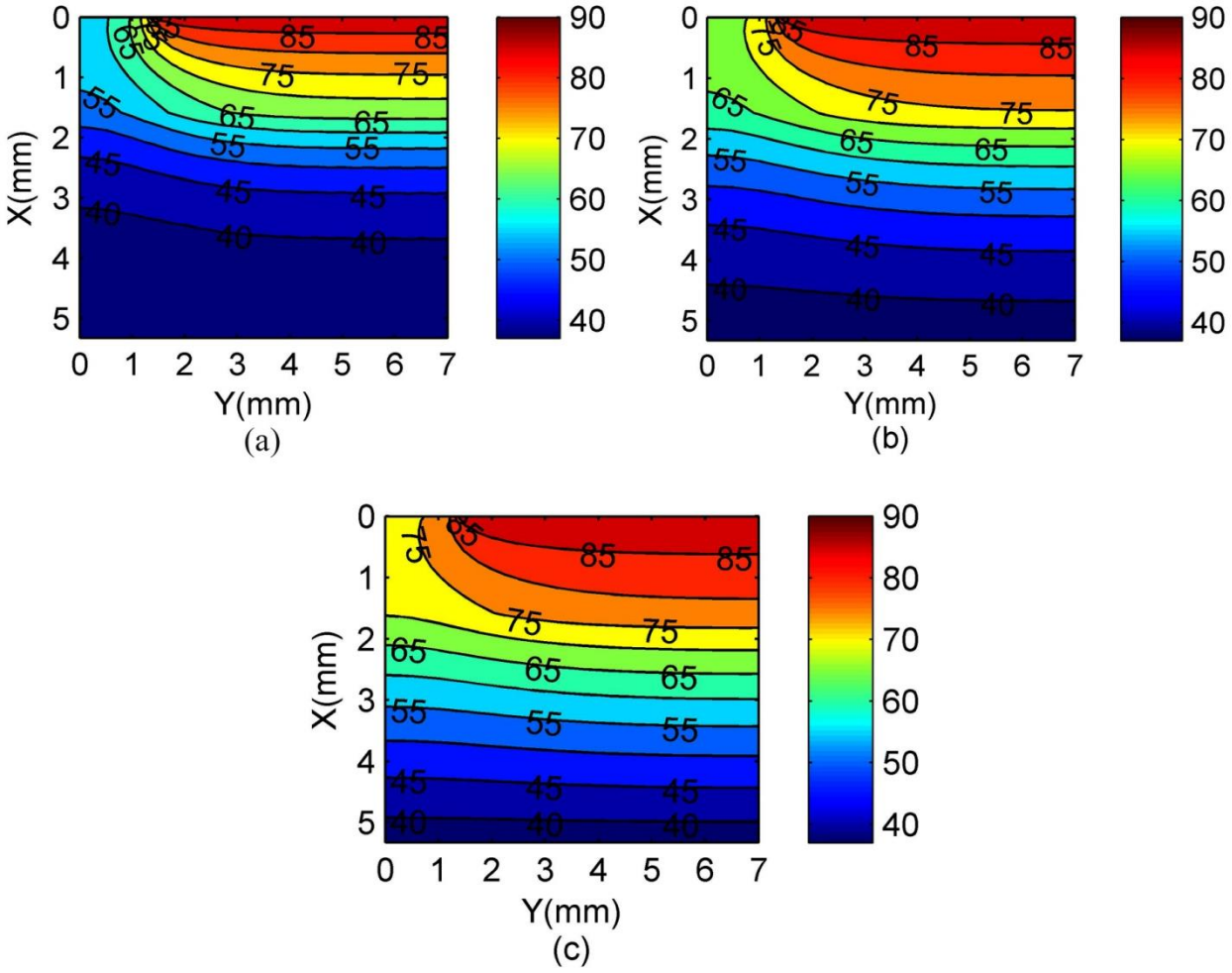

Figure 1.16 Temperature distribution inside the tissue after heating (a)15s (b)30s and (c) 60s

Fig. 4.16 shows the transient temperature distribution in human skin in case of heating with a hot disk. In our numerical analysis we consider three different heating times namely 15s, 30s and 60s respectively. Where Fig 4.16(a) shows the result after 15s heating and Fig 4.16(b) shows the result for 30s and Fig 4.16(c) for heating 60s. Here we assumed the disk temperature is 90^0C. The skin layers adjacent to the heating disk tend to increase its temperature faster due to the disk temperature. But the area which is not in contact with heating disk occupies lower temperature less than 78^0C. This lower temperature is obtained due to heat loss in that area by convection and evaporation to ambient air. After 15s heating the areas which are not in contact with heating disk is noticed lower temperature than 30s and 60s heating. After heating of these

three different times temperature of 45^0C penetrates 2mm, 3mm and 4mm depth respectively. As time passes more heat is distributed from the heating disk to towards body core.

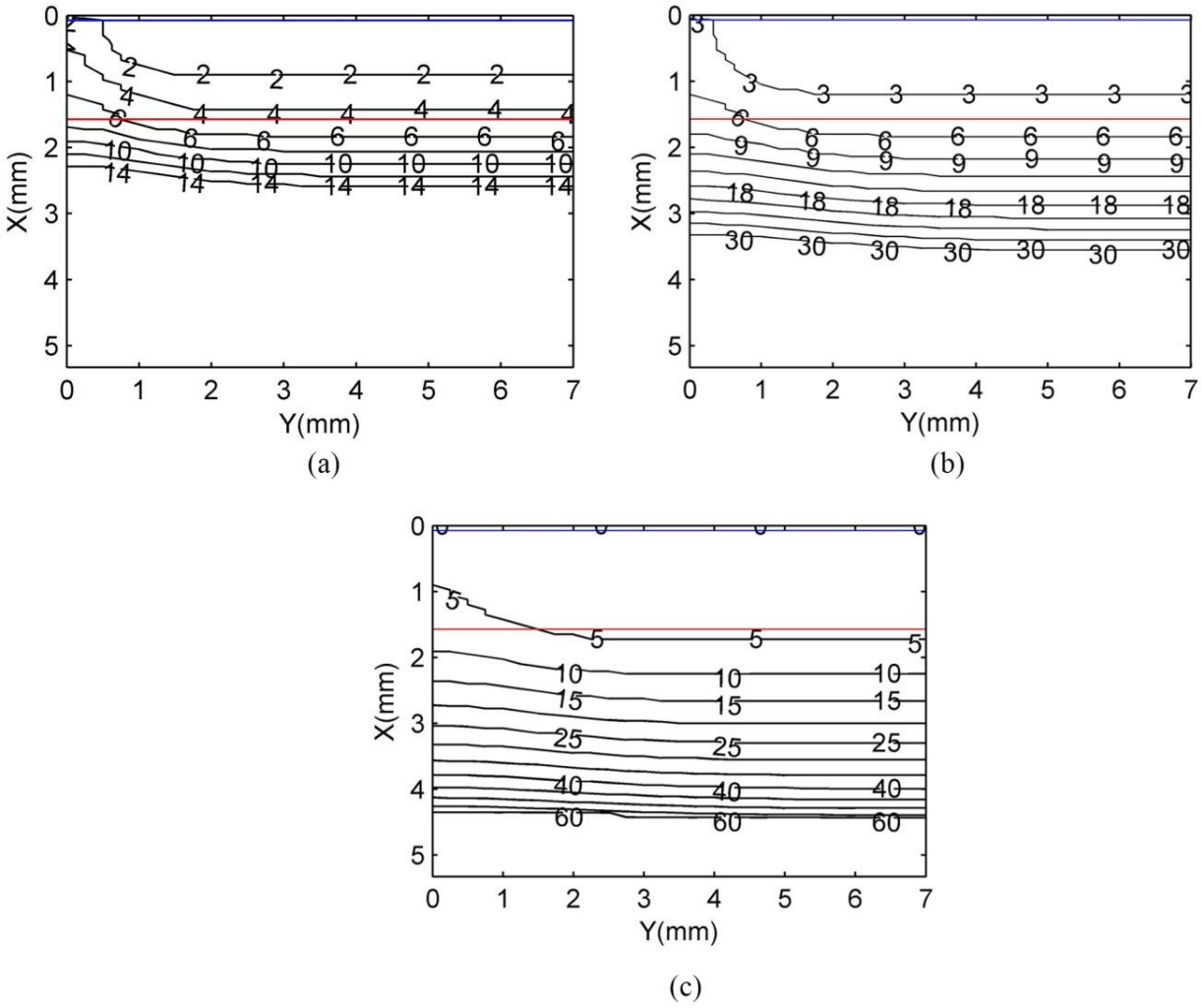

Figure 1.17 Development of 43^0C isotherm through the tissue after heating (a)15s. (b)30s. and (c) 60s

As scientists and researchers suggests that human tissue can undergo upto 43^0C without any damage[55]. So it is conveninent to know the time needs to reach that point. Fig. 4.17 illustrates the time contour for reaching 43^0C isotherm. Here the tissue above the blue line is the epidermis and the region below blue line and above the red line is the dermis region. It is showing that it takes only three second to start damage into the epidermis region and few portion of the dermis region. Almost 5s to reach on the whole dermis region except the region which is not in contact with the heating disk. As mentioned earlier this region undergoes

comparatively low temperature due to heat loss by convection and evaporation. Which results in lower damage in that region. Moreover if we increase the heating time upto 30s it penetrates further deeper. And after 60s it goes further than 4mm depth.

CHAPTER FIVE
COMPUTED HUMAN SKIN BURN INJURY

In this chapter, our finite element code will be used to calculate the temperature distribution of human skin under different boundary conditions. As the human skin has three different layers heaving distinct thermal properties our developed finite element model will handle inhomogeneity. We will get the time-temperature database using our computer code and using Henriques Burn Integral we will calculate the appropriate conditions of burn. Burn index relationship with distance, time, temperature and fraction of tissue damage will be investigated in this chapter. Finally, effect of cooling medium in skin tissue is explained.

5.1 Burn Quantification

The development of injury is predicted from the calculated temperature-time history by using the Henriques damage function.

$$\frac{\partial \Omega}{\partial t} = \int_0^t P e^{\frac{-\Delta E}{RT}} dt \qquad (5.1)$$

By integrating with respect to time *t*, we get

$$\Omega = P \exp(-\frac{\Delta E}{RT})t$$

From our finite element model we get the transient time-temperature database and using this equation we measure the value of Ω. It was found that 1st degree burn occurs when Ω = 0.53, for second degree burn Ω =1 & for third degree burn $\Omega = 10^4$.In our study, the pre-exponential value and activation energy used as P= $3.1\times10^{98}[S^{-1}]$ and ΔE= $6.03\times 10^5[Jmol^{-1}]$[55,56]. It was found that 1st degree burn occurs when Ω=0.53, for second degree burn Ω=1 & for third degree burn $\Omega=10^4$. Numerical values of individual parameters as used in the study are presented in Table 4.1.

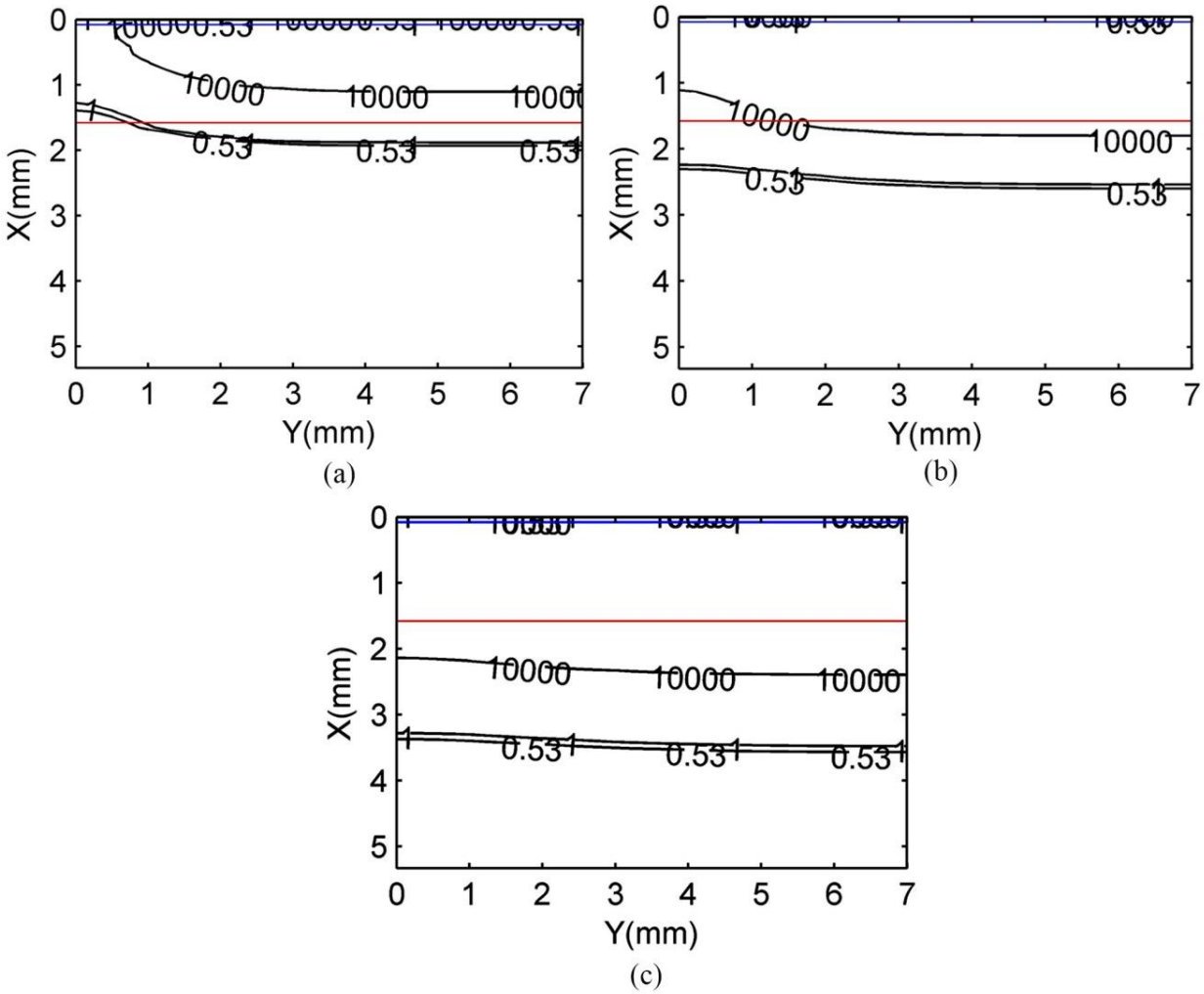

Figure 2.1: Damage index profile after heating (a)15s (b)30s and (c) 60s

Injury profile after 15s heating is shown in Fig 5.1(a). Where Fig 5.2 (b) and Fig 5.3 (c) shows the injury profile respectively after 30s and 60s heating. From this figure 1st degree burn line (0.53 level) and 2nd degree burn line (1 level) is very close to each other. This reveals that after attaining 1st degree burn it occupies to 2nd degree burn rapidly. But relatively it takes more time to reach 3rd degree burn. After 15s heatinng 1st degree and 2nd degree burn covers the whole epidermis and dermis region and starts to get into deeper. And 3rd degree burn covers the whole epidermis and few portion of the dermis region. But after heating 30s 1st degree and 2nd degree burn spreads towards the fat region after the epidermis and dermis region. The epidermis region is fully vanished as 3rd degree burn presents here and most of the part of the dermis region also

destroyed as the presence of 3rd degree burn. A few portion of the fat region also notice the presence of 3rd degree burn.

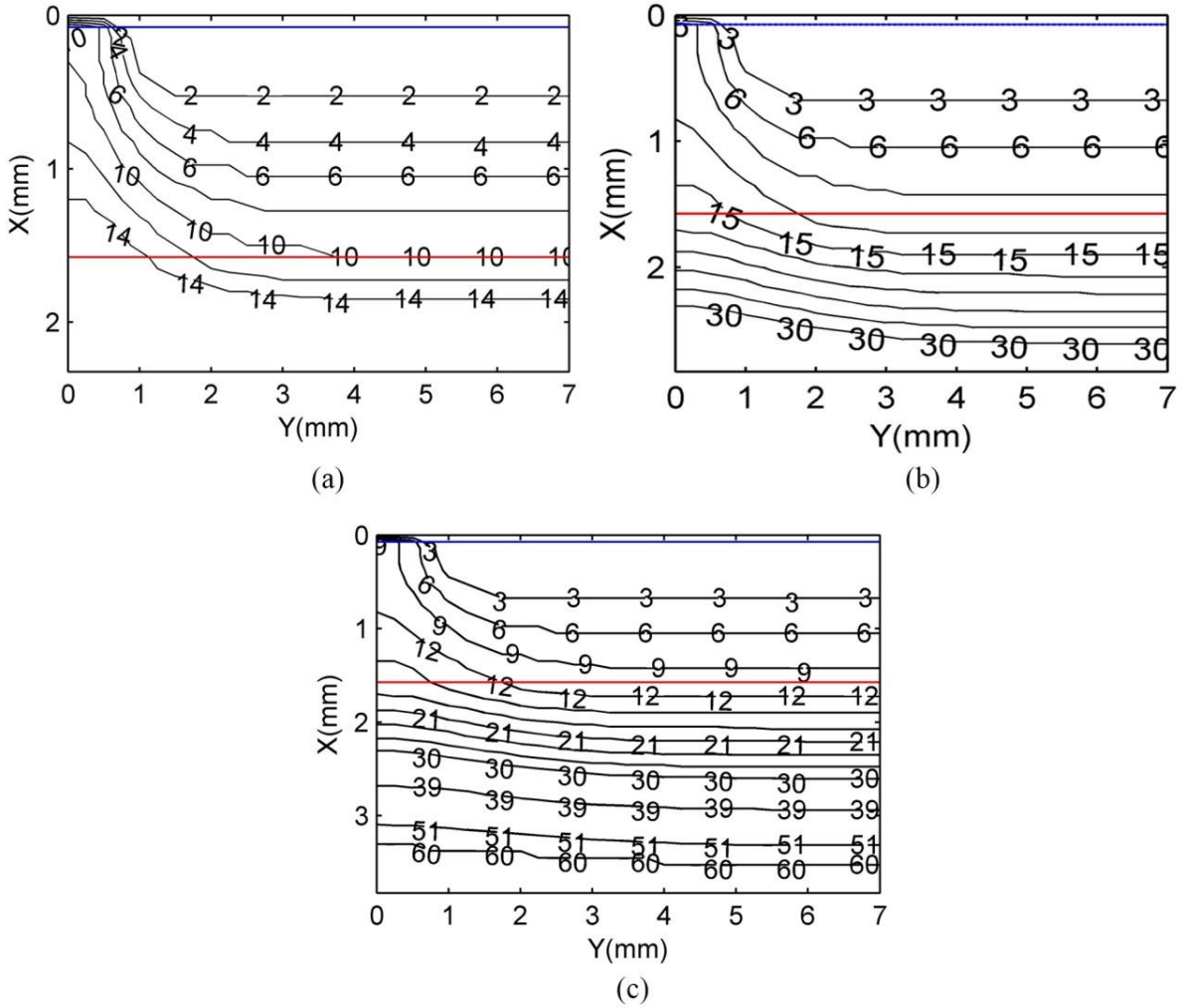

Figure 2.2 Time to attain 1st degree burn after heating (a)15s (b)30s and (c) 60s

Where after 60s heating whole epidermis, dermis as well as some parts of the fat region is affected by the third degree burn.1st and 2nd degree burn goes more than 3mm depth from the skin surface.

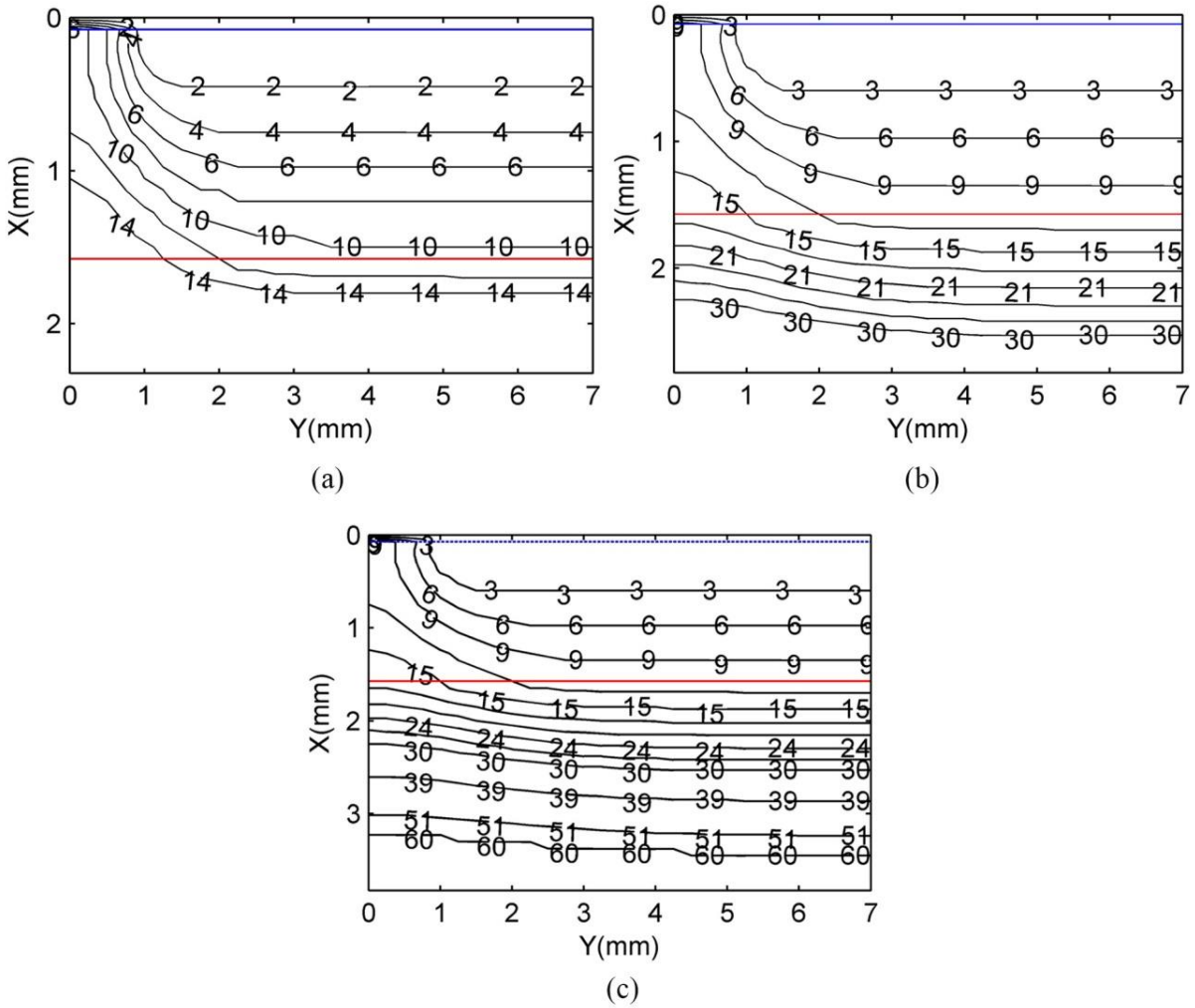

Figure 2.3 Time to attain 2nd degree burn after heating (a)15s (b)30s and (c) 60s

Advances of the 1st degree burn is shown in Fig 5.2. Where 2nd and 3rd degree burn advancement are showing in Fig 5.3 and Fig 5.4. Significant difference is not found in Fig 5.2 and Fig 5.3. This is because as mentioned earlier 1st degree burn exist for very short time and reaches to higher degree burn immediately.From Fig 4.17(a) we noticed that after 14s damage starts beyond x = 2mm line. But from Fig 5.2(a) it is showing that after 14s burn exists before x=2mm line although at that time damage stars after that region.

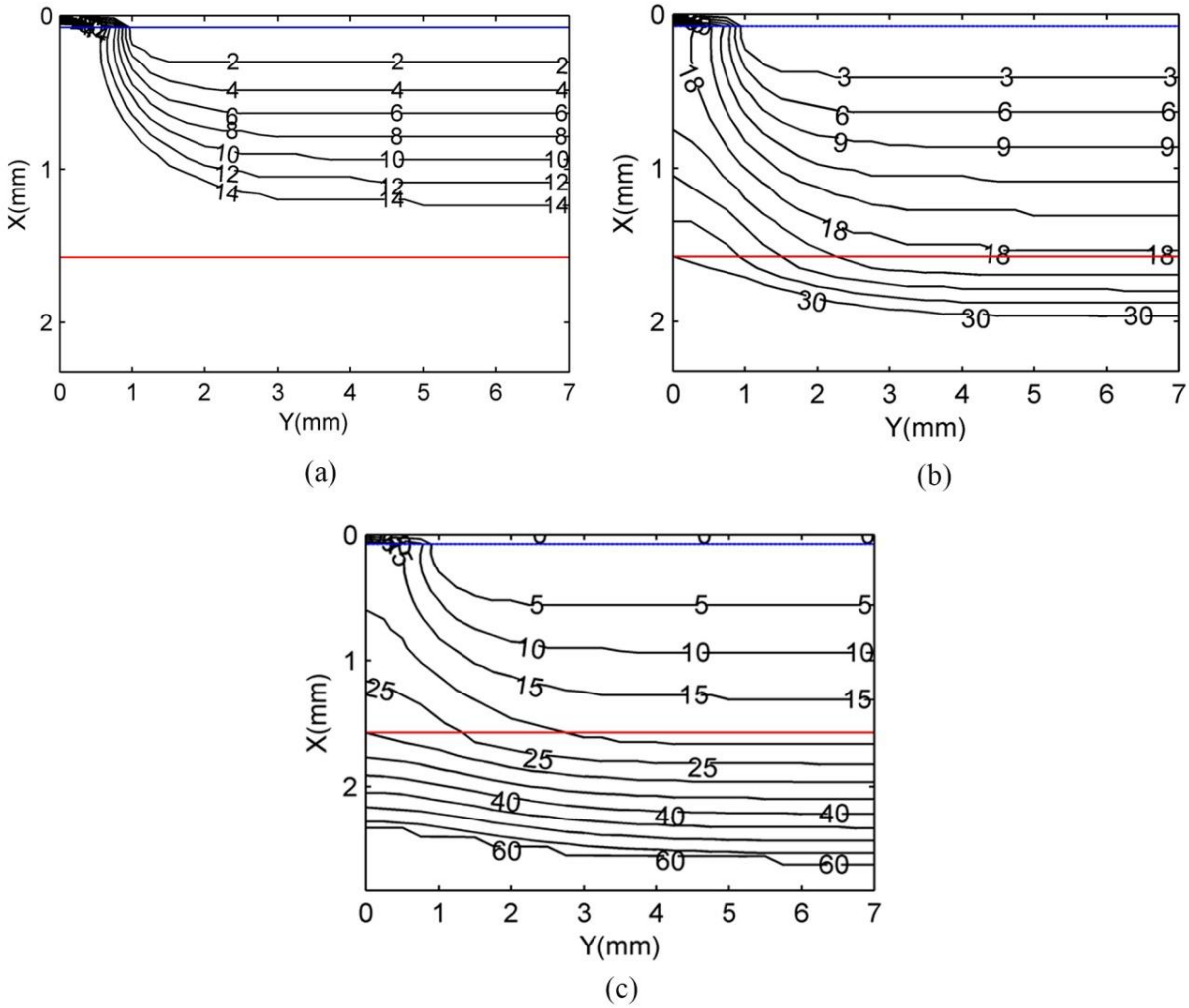

Figure 2.4 Time to attain 3rd degree burn after heating (a)15s (b)30s and (c) 60s

So after attaining the damage threshold value burn does not starts although at that time cell dagame starts. It takes relatively more time to obtain 1st degree burn after tissue reaching damage threshold valiue. This statement is also shown in injury profile figure at Fig 5.1(b). But After 30s, 2nd degree burn reaches behind the x=2mm line and after 60s heating 1st and 2nd degree burn reaches to 3mm depth.

Fig 5.4 shows the penetration of the 3rd degree burn over time. There are significant difference among Fig 5.4, Fig 5.3 and Fig 5.2. Third degree burn occures more lately after 1st and 2nd degree burn. As third degree burn is very dangerous, it destroys full epidermis and dermis region and sometimes reaches to the bones also, that's why it needs more time.

After 15s heating third degree burn covers the epidermis and almost most of the dermis region. After 60s heating it covers the whole dermis region and advances towards the fat region. And after 60s heating few portion of the fat region is affected by the 3rd degree burn. But like as Fig 2, Fig 5.1, Fig 5.2 and Fig 5.3 it is clear from Fig 5.4 that due to heat loss from convection and evaporation the bare protected by heat convection and evaporation from third degree burn. Both injury and degrees of burn delayed to reach that region.

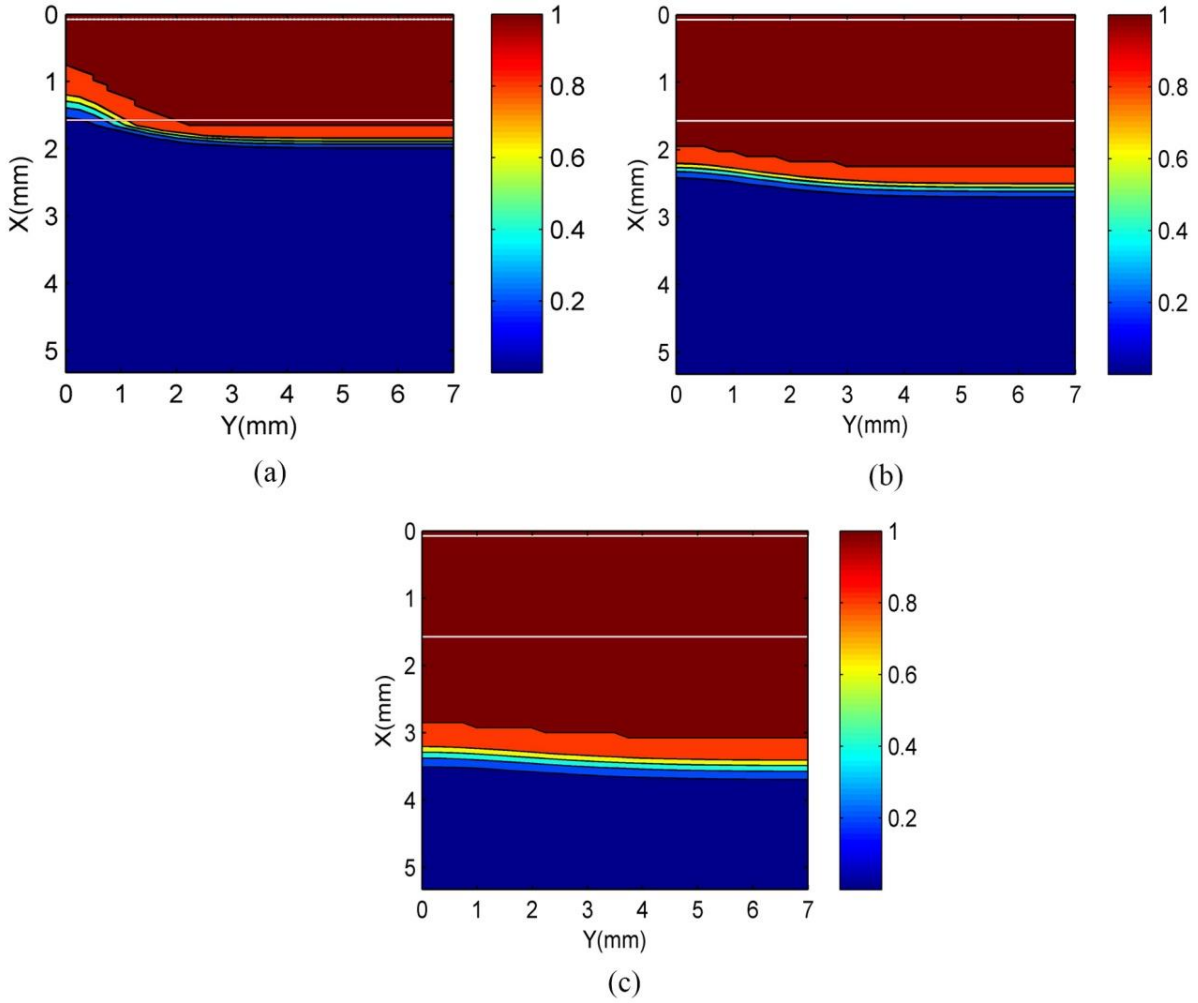

Figure 2.5 Fraction of tissue damage after heating (a) 15s; (b) 30s; (c) 60s

The fraction of tissue damage can be shown as fig 5.5. Fraction of tissue damage calculated by the following equation:

$$\theta = 1 - exp\ (-\Omega)$$

Here θ is scaling from 0 to 1. One means completely destroy the affected tissue. After 15s of heating notice that epidermis and dermis region vanishes completely except the region which is not direct contact of heating disk. This is because some heat passes through this region to the ambient. From fig 5.5(b) seems that epidermis and dermis and some part of fat region destroy and goes to beyond x = 2mm depth. We notice from fig 5.5(c) the tissue damage goes to x = 3mm depth from skin surface. The fraction of tissue damage increases with exposure of time. So, it is very important to know the duration of exposure time and temperature to predict the damage of the tissue.

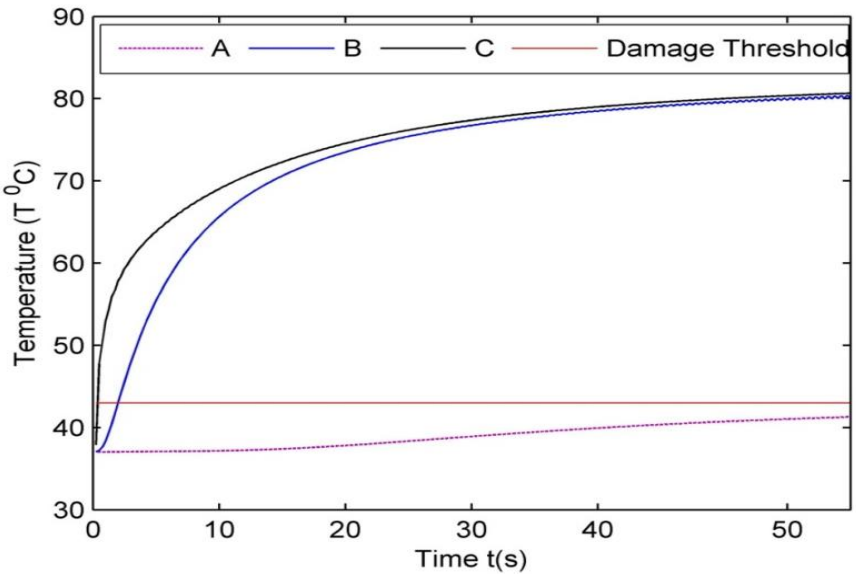

Figure 2.6 Temperature along time at three different points.

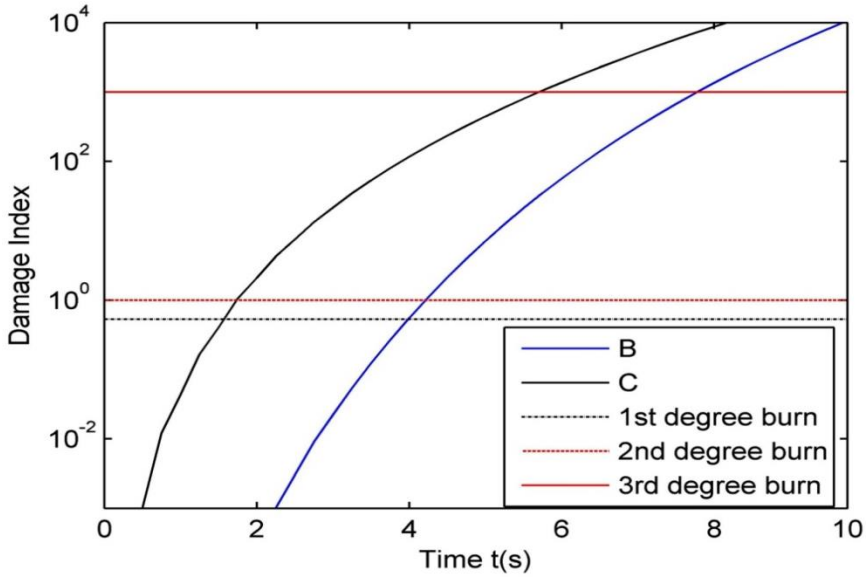

Figure 2.7 Damage index along time at three different points. (Curve A, Curve B and C)

Figure 5.6; shows the temperature distribution inside human tissue at three different points A(4.7893, 0), B(1.2750, 4.0), and C(0.150, 1.0) respectively. Fig. 5.7 demonstrates the corresponding damage index at these points. Temperature increases with respect to time. But point C and point B achieves higher temperature than point A. Moreover temperature of point C is higher than point B. This difference happens as the position of the points and heating disk. This means that close proximity to heating disk is more temperature. As point A is located further than point B and C, its temperature is lower than other points.

However, from Fig 5.6 where it is showing that temperature of point A does not crosses the damage threshold temperature. It reflects on the damage index value in Fig 5.7. Where shows that value of damage index remains 0 at all time. But in case of Curve B and Curve C as their temperature goes further the damage threshold value there damage index increases exponentially along time. Moreover it takes more time to reach 1st degree, 2nd degree and third degree burn of curve B than Curve C. As curve C is closer to heating disk than curve B.

5.2 Effect of surface cooling

In this case, after exposing to hot disk ($T=90^0C$ &h_f= $7W/(m^2.^0C)$) up to a certain period (15s) cooling medium is used to reduce the tissue temperature. As different cooling medium has different heat transfer coefficient so it is necessary to know the effect of cooling medium heat transfer coefficient.

From Fig 5.8 it is clear that when surface cooling is applied temperature drops sufficiently. Depending upon the time, temperature and heat transfer coefficient of cooling medium tissue temperature may reach below the core temperature (37^0C). The following figures show that cooling medium drops the tissue temperature quickly immediately after applying, but as time increases the cooling rate decreases. It is for the reason that as time goes temperature gradient between tissue temperature and coolers decreases which results in low cooling.

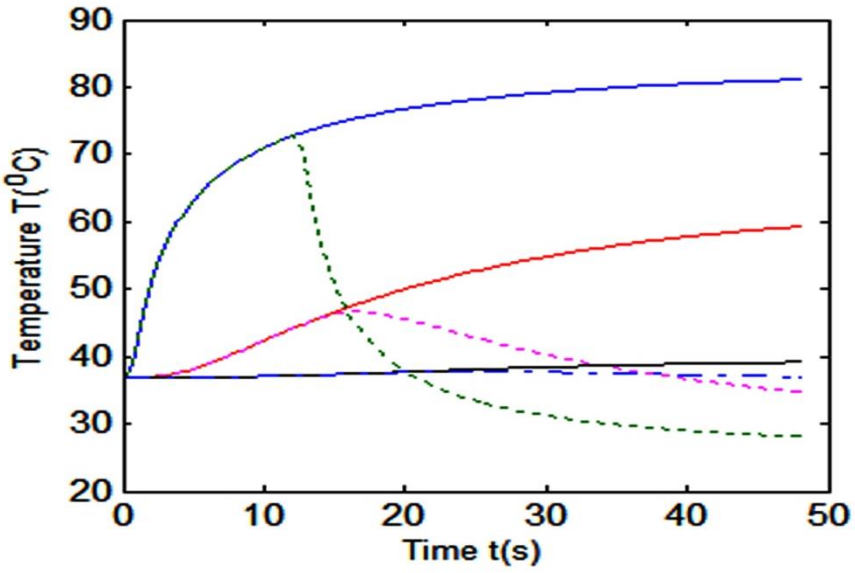

Figure 2.8 Effect of subsequent cooling after heating via heating disk at three different points.

Simulations are carried out to predict the temperature distribution inside the skin model when heated 15s at constant temperature and then using cooling medium. This figure shows the temperature distribution of skin tissue at three different points. Three lines whose temperature

increases with time represent the temperature 15s of constant heating. After 15s, the heating disk is removed and cooling pad is setup on the skin. Here noticed that temperature of these three points declined with time due to cooling pad. The dotted lines represent the temperature of these points.

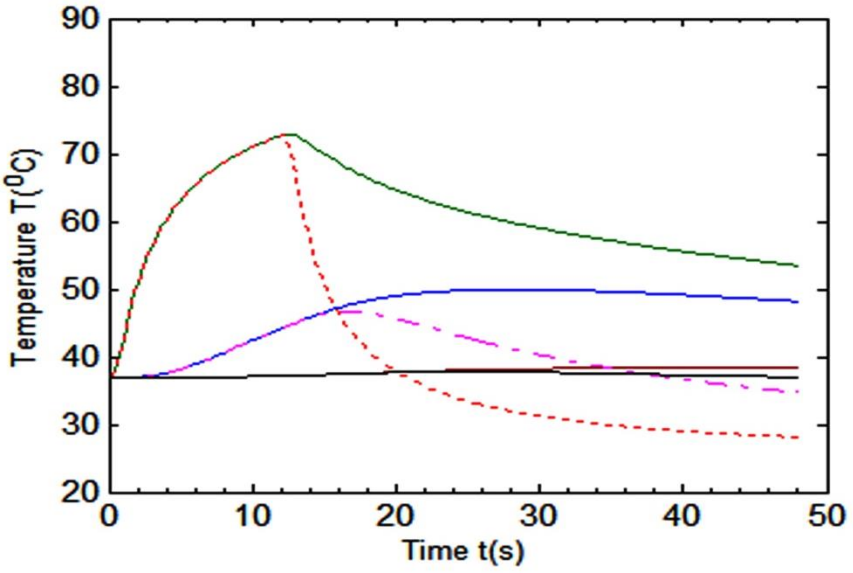

Figure 2.9 Results of two different cooling procedures after heating at three different points.

Fig. 5.9 shows the temperature distribution of skin tissue in three situations. First 15s shows the tissue temperature with constant heating disk. Then we remove heating disk. We notice the tissue temperature decrease slowly with time. The solid lines stand this value in three different points. It takes relatively more time to reach the body core temperature at 37^0C. The dotted lines represent the value of tissue's temperature after introducing the cooling pad. The decline rate of tissue temperature is faster when cooling pad is placed on the skin surface.

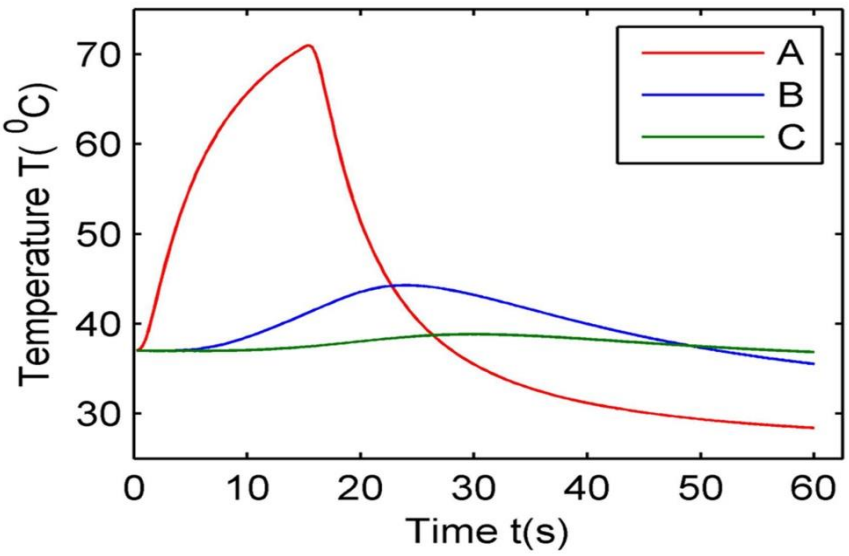

Figure 2.10 Reduction of tissue temperature as heating disk is removed and cooling pad is placed.

Fig. 5.10 shows the temperature distribution of skin tissue at three different points. First 15s temperature increased exponentially which point is near to the skin surface represent the red line. After setup the cooling pad, the temperature decreased dramatically at the same point. This is because closed point to the skin surface gain and lose heat faster than other points. The point B and C far away from the skin surface which represent the blue line and green line. Here we noticed that blue line temperature increased slowly from 10s to 25s then fall gradually. At point C we have not seen a significant effect of temperature change because this point is near to the body core. We can draw a conclusion from this figure after affected skin burn if we introduce immediately cooling pad, we may protect the skin tissue from major injury.

Fig.5.11 demonstrates the contour plot of temperature gradient of 30s of heating hot disk and cooling pad. It has been noticed that the maximum temperature is 44^0C which is very close to the threshold value of burn 43^0C. As a result, after 15s of cooling pad there is no damage propagated in the skin tissue. If we want to get the optimum benefit of cooling pad, it has been better to set up cooling pad within 15s of burn.

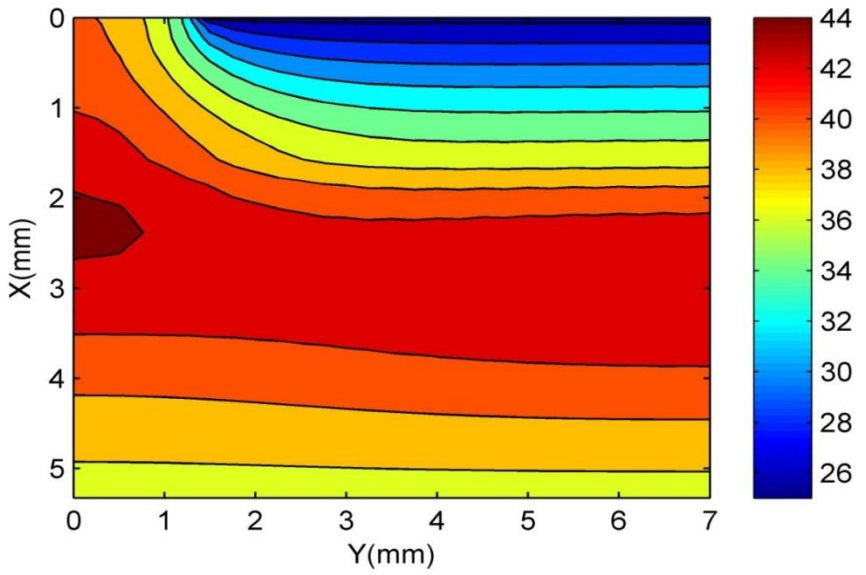

Figure 2.11 Temperature contour of cooling using cooling pad after heating for 15s.

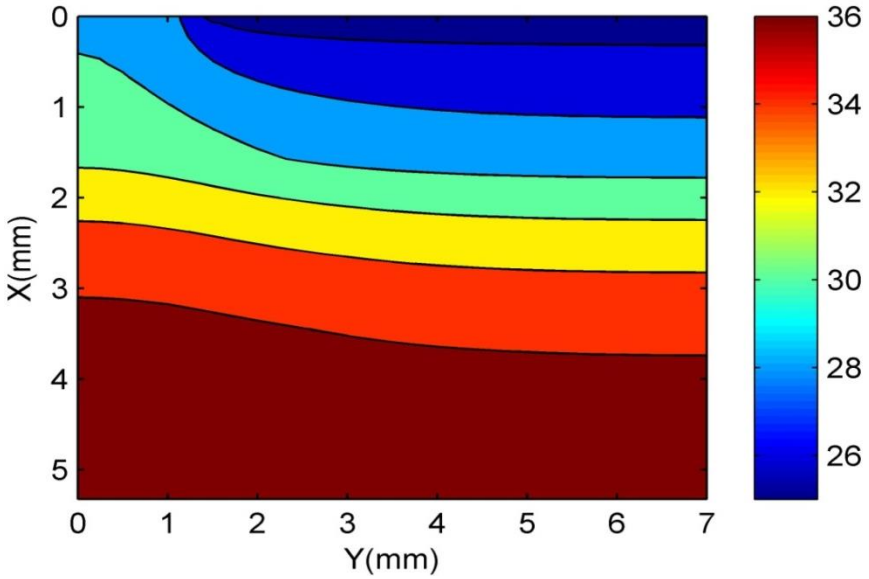

Figure 2.12 Temperature contour of cooling by cooling pad for 45s after heating 15s.

Fig.5.12 shows the predicted temperature distribution inside the skin using the control parameters presented in Table 4.1. Simulations are carried out for first 15s of constant heating disk and next 45s of using cooling medium. The lowest temperature happens in the whole

domain of the skin which is less than at body core temperature of 37^0C.The solid lines in Fig.5.12 indicate the isotherms inside the human skin.

CHAPTER SIX
CONCLUSION AND RECOMMENDATIONS

6.1 Conclusion

For the study of heat transfer profile in human tissue finite element model of Pennes bio-heat equation is developed in this study. Related computer code using programming language C is developed to calculate the results. Our computed results are compared with analytical and COMSOL-Mutiphysics results which agrees strongly with the accuracy. Results obtained under different heating and cooling conditions appear in practical cases. From these results the following conclusions can be made:

- In surface heating higher temperature develops at the skin surface and temperature decreases along with distance. This type of heating will be efficient approach for treating cells locate near the skin surface.
- Due to stochastic behavior of the environmental temperature or external heating the tissue temperature fluctuates within a very narrow range thus there is no possibility of arising danger in such case.
- Cell damage increases exponentially along with time, temperature and heat flux but it decreases exponentially along with distance from the skin surface.
- Burn decreases along with distance from the skin surface. Burn occurs mainly in the epidermis area. It takes very little time to destroy all cells, soon after the start of the damage. Depending upon the nature of the exposure the duration varies.
- Subcutaneous thermal conductivity has a significant effect on the tissue temperature. The dermis layer effect is less significant and the effect of epidermis is almost negligible.
- After exposing to flame or hot fluid, exposing to cold fluid will be an efficient approach to reduce tissue temperature. But it cannot reduce the amount of burn that already occurred. Moreover, it can prevent from further burn.
- The models described in this study could be useful for the researchers and medical scientists to improve the diagnosis and treatment. Results described in this study could

be useful to accurately predict the thermal behavior of living tissues and can be extended to such application as parameter estimation, clinical treatment and medical protocols design and to optimize for surgical treatment.

6.2 Recommendation for Further Study

1. 2D problem is covered in this study. Three dimensional problems can be considered in the future work.
2. Phase change during heat transfer does not consider in this study, this can be added in future study.
3. Non-linear bio heat transfer model can be solved as further study.

Reference

1 Pennes, H. H. Analysis of tissue and arterial blood temperatures in the resting human forearm. *J Appl Physiol* **1**, 93-122 (1948).

2 He, Y., Shirazaki, M., Liu, H., Himeno, R. & Sun, Z. A numerical coupling model to analyze the blood flow, temperature, and oxygen transport in human breast tumor under laser irradiation. *Computers in Biology and Medicine* **36**, 1336-1350, doi:https://doi.org/10.1016/j.compbiomed.2005.08.004 (2006).

3 Ng, E. Y., Tan, H. M. & Ooi, E. H. Prediction and parametric analysis of thermal profiles within heated human skin using the boundary element method. *Philos Trans A Math Phys Eng Sci* **368**, 655-678, doi:10.1098/rsta.2009.0224

368/1912/655 [pii] (2010).

4 Torvi, D. A. & Dale, J. D. A finite element model of skin subjected to a flash fire. *J Biomech Eng* **116**, 250-255 (1994).

5 Viglianti, B. L., Dewhirst, M. W., Abraham, J. P., Gorman, J. M. & Sparrow, E. M. Rationalization of thermal injury quantification methods: application to skin burns. *Burns* **40**, 896-902, doi:10.1016/j.burns.2013.12.005

S0305-4179(13)00412-9 [pii] (2014).

6 Ng, E. Y. & Chua, L. T. Comparison of one- and two-dimensional programmes for predicting the state of skin burns. *Burns* **28**, 27-34, doi:S0305417901000663 [pii] (2002).

7 Kohani, M., Talebi, M. & Shafii, M. *Modeling and optimizing the temperature distribution around cancerous tissues during magnetic hyperthermia treatment*. (2012).

8 Javidi, M. *et al.* Evaluation of the Effects of Injection Velocity and Different Gel Concentrations on Nanoparticles in Hyperthermia Therapy. *Journal of Biomedical Physics & Engineering* **4**, 151-162 (2014).

9 Mizera, A. & Gambin, B. Modelling of ultrasound therapeutic heating and numerical study of the dynamics of the induced heat shock response. *Communications in Nonlinear Science and Numerical Simulation* **16**, 2342-2349, doi:https://doi.org/10.1016/j.cnsns.2010.04.056 (2011).

10 Liu, H.-L., Chen, Y.-Y., Yen, J.-Y. & Lin, W.-L. THERMAL LESION FORMATION AND DETERMINATION FOR EXTERNAL ULTRASOUND THERMAL THERAPY. *Biomedical Engineering: Applications, Basis and Communications* **15**, 124-132, doi:10.4015/s1016237203000195 (2003).

11 Xu, F., Lu, T. J. & Seffen, K. A. Biothermomechanical behavior of skin tissue. *Acta Mechanica Sinica* **24**, 1-23, doi:10.1007/s10409-007-0128-8 (2008).

12 Shen, W., Zhang, J. & Yang, F. Modeling and numerical simulation of bioheat transfer and biomechanics in soft tissue. *Mathematical and Computer Modelling* **41**, 1251-1265, doi:https://doi.org/10.1016/j.mcm.2004.09.006 (2005).

13 Dhar, P., Dhar, R. & Dhar, R. An optimal control problem on temperature distribution in tissue by induced microwave.

14 Kaur, S. & Maini, S. Microwave Radiation—Therapeutic Application for Cure of Liver Tumor.

15 Chiaknjuri, V. R. *Heat Transfer Model for Cryosurgery*, (2011).
16 Yeung, C. J. & Atalar, E. A green's function approach to local rf heating in interventional MRI. *Medical physics* **28**, 826-832 (2001).
17 Deng, Z.-S. & Liu, J. Analytical study on bioheat transfer problems with spatial or transient heating on skin surface or inside biological bodies. *Journal of biomechanical engineering* **124**, 638-649 (2002).
18 Sharma, P., Ali, S. & Katiyar, V. Transient heat transfer analysis on skin surface and inside biological tissue. *Int J Appl Math Mech* **5**, 36-47 (2009).
19 Karaa, S., Zhang, J. & Yang, F. A numerical study of a 3D bioheat transfer problem with different spatial heating. *Mathematics and Computers in Simulation* **68**, 375-388 (2005).
20 Ooi, E., Ang, W.-T. & Ng, E. Bioheat transfer in the human eye: a boundary element approach. *Engineering Analysis with Boundary Elements* **31**, 494-500 (2007).
21 Chan, C. L. Boundary element method analysis for the bioheat transfer equation. *ASME J. Biomech. Eng* **114**, 358-365 (1992).
22 Scott, J. A. A finite element model of heat transport in the human eye. *Phys Med Biol* **33**, 227-241 (1988).
23 Scott, J. A. The computation of temperature rises in the human eye induced by infrared radiation. *Phys Med Biol* **33**, 243-257 (1988).
24 Desai, C. S. & Kundu, T. *Introductory finite element method*. (CRC Press, 2001).
25 Geng, J., Yan, W. & Xu, W. *Application of the finite element method in implant dentistry*. (Springer Science & Business Media, 2008).
26 Diller, K. R. Analysis of skin burns. *Heat transfer in medicine and biology: analysis and applications* **2**, 85-134 (1985).
27 Marieb, E. N. & Hoehn, K. The integumentary system. *Human Anatomy and Physiology. 8th ed. San Francisco, CA: Benjamin Cummings* **155** (2010).
28 Anthony, C. P. & Thibodeau, G. A. *Text Book of Anatomy and Physiology*. 10th edn, pp. 70-73, 290-294, 530-533

(Mosby, 1979).
29 Torvi, D. A. A finite element model of heat transfer in skin subjected to a flash fire. (1993).
30 Henriques Jr, F. & Moritz, A. Studies of thermal injury: I. The conduction of heat to and through skin and the temperatures attained therein. A theoretical and an experimental investigation. *The American journal of pathology* **23**, 530 (1947).
31 Moritz, A. R. & Henriques Jr, F. Studies of thermal injury: II. The relative importance of time and surface temperature in the causation of cutaneous burns. *The American journal of pathology* **23**, 695 (1947).
32 Moritz, A. Studies of thermal injury: III. The pathology and pathogenesis of cutaneous burns. An experimental study. *The American journal of pathology* **23**, 915 (1947).
33 Henriques Jr, F. Studies of thermal injury; the predictability and the significance of thermally induced rate processes leading to irreversible epidermal injury. *Archives of pathology* **43**, 489-502 (1947).
34 Buettner, K. Effects of extreme heat and cold on human skin. I. Analysis of temperature changes caused by different kinds of heat application. *Journal of Applied Physiology* **3**, 691-702 (1951).

35 Buettner, K. Effects of extreme heat and cold on human skin. II. Surface temperature, pain and heat conductivity in experiments with radiant heat. *Journal of Applied Physiology* **3**, 703-713 (1951).

36 Buettner, K. Effects of Extreme Heat and Cold on Human Skin III. Numerical Analysis and Pilot Experiments on Penetrating Flash Radiation Effects. *Journal of Applied Physiology* **5**, 207-220 (1952).

37 Lipkin, M. & Hardy, J. D. Measurement of some thermal properties of human tissues. *Journal of Applied Physiology* **7**, 212-217 (1954).

38 Hardy, J. D., Wolff, H. G. & Goodell, H. Studies on pain. A new method for measuring pain threshold: observations on spatial summation of pain. *Journal of Clinical Investigation* **19**, 649 (1940).

39 Mehta, A. & Wong, F. (MIT, Cambridge, Massachusetts, 1973).

40 Takata, A., Rouse, J. & Stanley, T. Thermal analysis program. *IIT, Chicago* (1973).

41 Wu, Y. A modified criterion for predicting thermal injury. *National Bureau of Standards, Washington* (1982).

42 Stoll, A. M. & Greene, L. C. Relationship between pain and tissue damage due to thermal radiation. *Journal of Applied Physiology* **14**, 373-382 (1959).

43 Ng, E., Tan, H. & Ooi, E. Boundary element method with bioheat equation for skin burn injury. *Burns* **35**, 987-997 (2009).

44 Diller, K. & Hayes, L. A finite element model of burn injury in blood-perfused skin. *Journal of biomechanical engineering* **105**, 300-307 (1983).

45 Wang, H. & Qin, Q.-H. A fundamental solution-based finite element model for analyzing multi-layer skin burn injury. *Journal of Mechanics in Medicine and Biology* **12**, 1250027 (2012).

46 Reddy, J. N. *An introduction to the finite element method*. Vol. 2 (McGraw-Hill New York, 1993).

47 Hedge, A. Thermal sensation and thermoregulation. *Lecture notes, Cornell University. See ergo. human. cornell. edu/studentdownloads/DEA350pdfs/thermreg. pdf* (2008).

48 Becker, E. B., Carey, G. F. & Oden, J. T. Finite Elements, An Introduction: Volume I. ., *258*, 1981 (1981).

49 Zienkiewicz, O. C., Taylor, R. L. & Taylor, R. L. *The finite element method*. Vol. 3 (McGraw-hill London, 1977).

50 Bald, W. New technique for determining thermal history and concentration gradients in biological specimens during cryopreservation, cryosurgery and ultrastructural studies. *CRYO-LETTERS* **2**, 201-206 (1981).

51 Peskin, C. S. Numerical analysis of blood flow in the heart. *Journal of computational physics* **25**, 220-252 (1977).

52 Rubinsky, B. & Cravahlo, E. G. A finite element method for the solution of one-dimensional phase change problems. *International Journal of Heat and Mass Transfer* **24**, 1987-1989, doi:https://doi.org/10.1016/0017-9310(81)90121-6 (1981).

53 Hayes, L. J. & Diller, K. R. A finite element model for the exposure of a composite man with distributed internal heat generation to a convective subfreezing environment. *ASME Paper* (1981).

54 Douglas, J., Jim & Dupont, T. Galerkin methods for parabolic equations. *SIAM Journal on Numerical Analysis* **7**, 575-626 (1970).

55 Diller, K. & Klutke, G. Accuracy analysis of the Henriques model for predicting burn injury. *Advances in Bioheat and Mass Transfer*, 117-123 (1993).
56 Diller, K. R. & Klutke, G.-A. Accuracy analysis of the Henriques model for predicting thermal burn injury. *ASME-PUBLICATIONS-HTD* **268**, 117-117 (1993).